Chapter 2

Chromium(III) Monodentate Nitrogen Ligand Chemistry

2.1 INTRODUCTION

The classes of compounds synthesised in this study belong predominantly to the chemistry of bidentate metal coordinated ligands which serve as a variation on the known successful catalytically active tridentate systems [32].

However, common to these classes of compounds is the addition of monodentate pyridine and derivatives thereof; these are expected to occupy the one remaining thf site around the metal centre of which the precursor molecule is $[CrCl_3(thf)_3]$.

Since its discovery in 1846 by Anderson [69], pyridine chemistry has played an important role in a wide array of chemical disciplines. This heterocyclic planar hexagonal framework is widely recognised for its stability and coordination capabilities. The former is a result of the delocalised π–electron cloud formed via sp^2 hybridisation, while the latter stems from the lone pair of electrons on the endocyclic nitrogen atom which aligns perpendicular to the ring system and is available for bonding to transition metals [70]. These factors, coupled with the ability to alter both the steric and electronic properties of the system via the addition of various substituents at the 2, 3 and 4 ring positions, were important in the selection of pyridine for this particular study. The recent work by McGuinness [42] on Cr(III) pyridyl–carbene complexes only served to confirm this selection as it illustrates that chromium(III)–pyridine chemistry is still very relevant.

It was therefore decided that it would be of benefit first to study the coordination of these monodentate ligands to the chromium metal centre. This resulted in novel crystallographic,

spectroscopic and computational insights which provided the perfect backdrop to the analysis of the bidentate systems that follow.

Although [CrCl$_3$(py)$_3$] **(3)** and [CrCl$_3$(pyphenyl)$_3$] **(8)** had been synthesised previously [71, 72], their synthetic routes differed and the studies lacked the additional characterisation and analytical insights provided by this study.

It is worth mentioning that pyridine chemistry and IR spectroscopy in particular are well suited since assignments are both straightforward and uncomplicated for a number of reasons. Firstly, the assignments of the vibrational modes of the free pyridine ligand have long since been known and so comparisons with complexes can be made in terms of the shifting of bands. This leads to a second simplifying feature. Only a small number of the internal vibrations of pyridine shift upon coordination to a metal centre, while the majority recur virtually band for band, with a few minor exceptions [73]. The bands that are affected shift by varying degrees relative to a number of factors, which include ligand substituents, type of metal, geometrical arrangements, etc. [74, 75].

Thirdly, the assignment of many metal–ligand vibrations in the IR region is complicated by the presence of ligand modes. This, however, is not the case in pyridine complexes as below 400 cm^{-1} no pyridine bands are visible, thus aiding M–L assignments [73].

Within this study there are three distinct categories. The first focused on the ability to control the sequential addition of the pyridine ligand to the precursor. The second involved an investigation based on steric hindrance and whether substituents at the ortho position of the pyridine would allow coordination via the endocyclic nitrogen to take place. The third category was the addition of three molar equivalents of the respective substituted pyridine ligands to the metal centre.

2.2   CATEGORY ONE: SEQUENTIAL ADDITION OF PYRIDINE

The ability to coordinate different monodentate ligands selectively and sequentially to the same [CrCl$_3$(thf)$_3$] precursor would provide a wide array of monomeric compounds with different steric and electronic properties. This was investigated through the addition of pyridine to

[CrCl$_3$(thf)$_3$] in thf in 1, 2 and 3 molar equivalents (see Figure 2.1) with the hope of extending the study to incorporate various substituted pyridines. A further reaction was carried out whereby pyridine was added to the chromium precursor in a large excess and, in fact, the pyridine acted as both ligand and solvent. Upon immediate addition of the ligands (regardless of the molar quantity), a dark green solution accompanied by an olive green precipitate was observed. The reactions were stirred overnight at room temperature to ensure completion.

On addition of the varying amounts of ligand, all four reactions turned green via a grey/blue intermediatory colour which was visible only for a matter of seconds and therefore was unable to be isolated. This is of importance as Elowe [38] discussed the relationship between dimers and such colours. In fact, the dimeric existence was indirectly proved for this category by one of the crystal structures that was determined during this investigation.
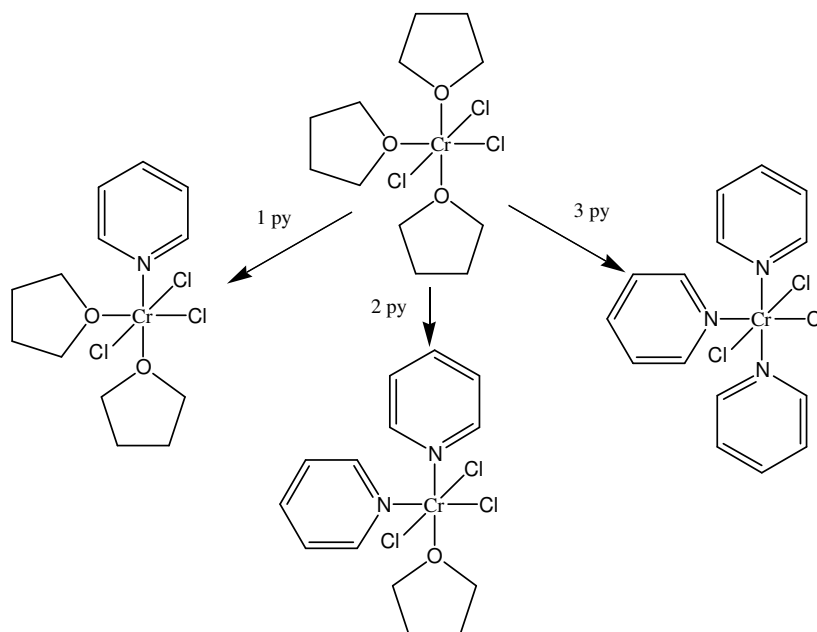
Figure 2.1   **Sequential addition of pyridine to the chromium precursor**

2.2.1 VISUAL ANALYSIS

This was the first technique to suggest similarities in the four complexes as all precipitates had the same olive green colour (Figure 2.2).

Figure 2.2   Olive green precipitate

2.2.2 INFRARED AND RAMAN SPECTROSCOPY

The results added further weight to the initial visual analysis and correlated well with the crystallographic structures of $[CrCl_3(py)_2(thf)]$ **(2)** and $[CrCl_3(py)_3]$ that follow, as the spectra of the different molar equivalents were virtually identical. In these spectral comparisons it is worth highlighting that the IR spectrum of the single crystal material was identical to the precipitate spectra. This indicates that the determined structure is representative of the bulk material.

 They all possess the expected vibrations associated with a pyridine ligand with respect to C–H and ring vibrations [73, 74]. A number of characteristic shifts relative to the free pyridine were also observed, which are recognised as being indicative of coordination to a metal centre [73, 74]. These are documented in Table 2.1 with the spectra of free pyridine and $[CrCl_3(py)_3]$ shown in Figure 2.3.

**Table 2.1   Characteristic pyridine shifts in the IR spectrum**

Free pyridine IR / cm^{-1}	$[CrCl_3(py)_3]$ IR / cm^{-1}	Shift / cm^{-1}
1582	1609	27
1438	1447	9
1029	1046	17
992	1014	22
746	763/754	17/8
604	640	36
404	445	41

Note that the values in the table are taken from the spectrum of $[CrCl_3(py)_3]$.
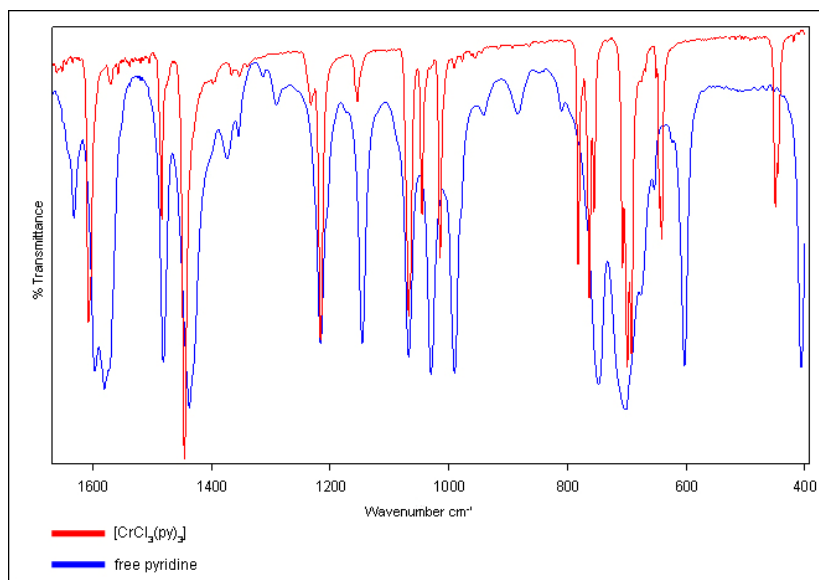
Figure 2.3 **Comparisons of the IR spectra of free pyridine (blue) and [CrCl₃(py)₃] (red)**

Although the Raman spectrum of $[CrCl_3(py)_3]$ was virtually identical to the IR spectrum, as illustrated in Figure 2.4 the intensities of the vibrations were noticeably different. One should be aware that although this is not entirely clear from the figure presented, there are in fact very weak vibrations at 783, 768 and 704 cm^{-1} which correspond to those exhibited in the IR spectrum.
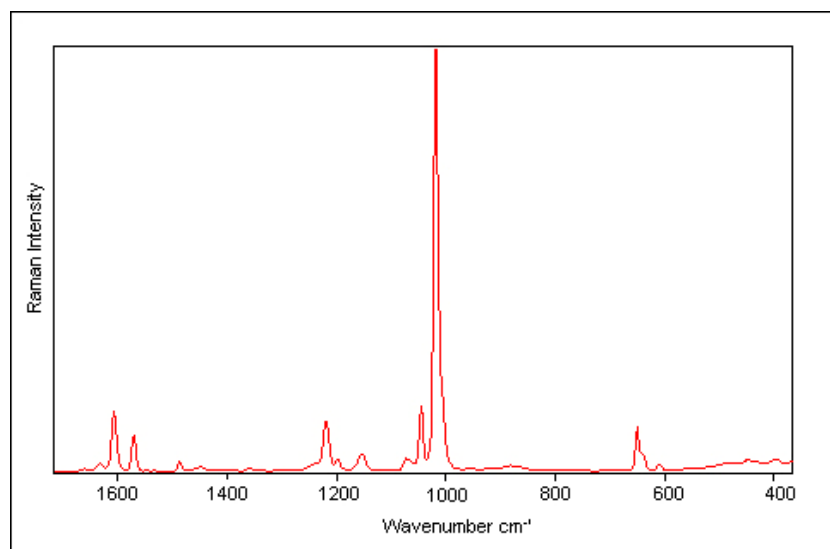
Figure 2.4 **Raman spectrum of [CrCl₃(py)₃]**

Worthy of particular mention is the shifting of the band at 992 cm^{-1} in free pyridine to 1014 cm^{-1} in the complex, as has been specifically highlighted in Figure 2.5. This is widely recognised as an indication of both bond strength and coordination, and is of particular interest in the study of the substituted pyridines as the degree of shifting is substituent dependent [75].
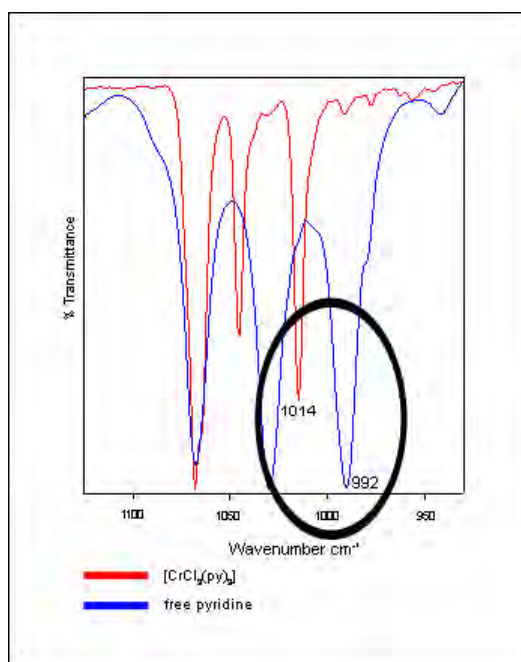

Figure 2.5   **Shifting of the free pyridine band (blue) in the IR spectrum at 992 cm^{-1} upon coordination (red)**

Relevant to this investigation is the absence of thf vibrations as it will aid the verification of tri-pyridine coordination. C–H vibrations of thf would have been expected around 2962-2925 cm^{-1} (lower than pyridine C–Hs [76]), while one of the most characteristic vibrations associated with coordinated thf (C–O–C) should have been observed as a strong IR vibration at ~856 cm^{-1} [77, 78].

The fact that none of these vibrations were observed in any of the compounds further confirmed the tri–pyridine coordination and thus the inability to control pyridine addition under these conditions.

Figure 2.6 highlights the presence of the characteristic thf–related vibrations in the [CrCl$_3$(thf)$_3$] precursor and their absence in [CrCl$_3$(py)$_3$].
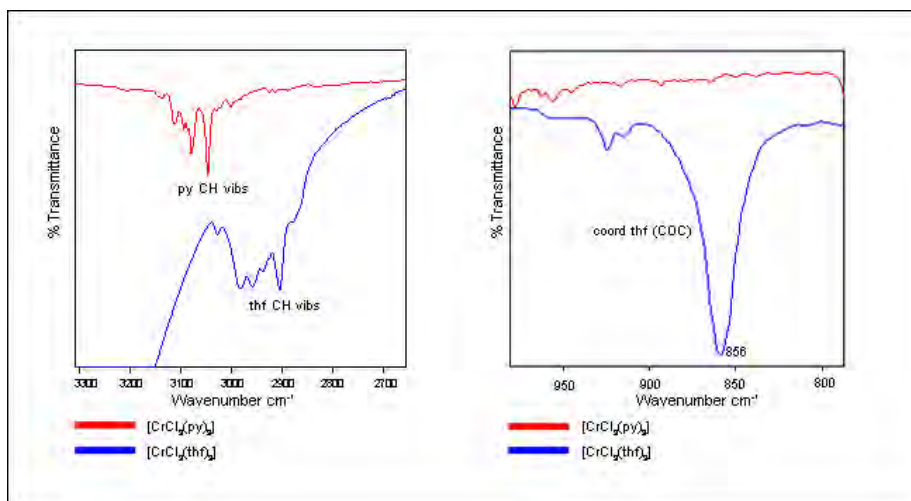
Figure 2.6   **Comparison between [CrCl$_3$(thf)$_3$] (blue) and [CrCl$_3$(py)$_3$] (red) IR spectra**

Furthermore, the molecular geometry observed in the crystallographic results was supported by the presence of three Cr–Cl vibrations which are indicative of the *mer* orientation [79]. They are visible between 390 and 310 cm^{-1} in all four compounds.

Perhaps most important is the assignment of the metal–ligand vibrations (Table 2.2). Clearly visible in [CrCl$_3$(py)$_3$] is the band at 221 cm^{-1} which corresponds to Cr–N of pyridine [41, 80, 81]. Unfortunately, the Cr–O of thf vibration is not as easy to assign but according to Fowles it may be the band observed at 284 cm^{-1} [82] and, as seen in Figure 2.7, this is absent in the spectrum of [CrCl$_3$(py)$_3$].
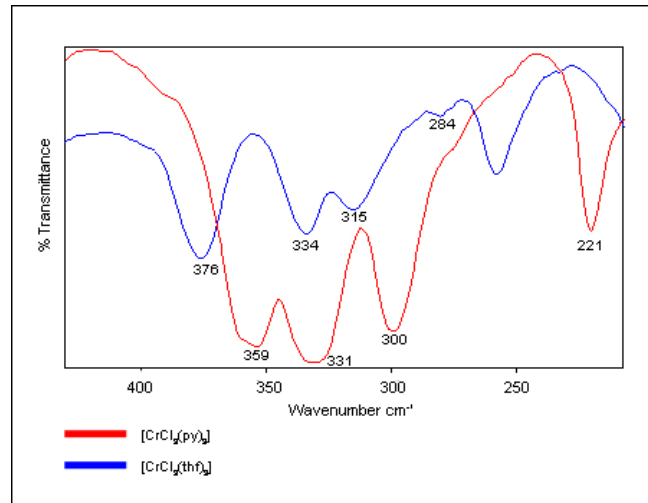
Figure 2.7   **FIR comparison between [CrCl$_3$(thf)$_3$] (blue) and [CrCl$_3$(py)$_3$] (red) spectra**

Table 2.2   Vibrational assignments of [CrCl$_3$(py)(thf)$_2$] (1), [CrCl$_3$(py)$_2$(thf)] (2), [CrCl$_3$(py)$_3$] (3)

| 1 IR / cm^{-1}	2 IR / cm^{-1}	3 IR / cm^{-1}	3 RAMAN / cm^{-1}	Assignment
3130m	3112m	3111w	3142w	ν (CH)
-	3078m	3079m	3079s	ν (CH)
3059m	3049m	3046m	3049m	ν (CH)
3030m	3028m	3030w	3030w	ν (CH)
1631m	-	-	1631w	ν_{ring}
1607s	1605s	1609s	1607m	ν_{ring}
1568m	1568w	1573w	1571m	ν_{ring}
1484s	1486m	1483m	1487w	ν_{ring}
1447s	1443s	1447s	1449w	ν_{ring}
1217s	1218s	1217s	1218m	δ (CH)
-	1148m	1153w	1152w	δ (CH)
1072s	1066s	1068s	1072w	δ (CH)
1045s	1045s	1046m	1046m	ν_{ring}
1015s	1014s	1014s	1018vs	Ring breathing (py)
-	-	781s	783vw	unassigned
756s	763s	763s 754m	768vw	γ (CH)
690s	698s	707s 699s 691s	704vw	γ (CH)
643s	642s	640s	650m 641sh	δ_{ring}
447s	449s	445s	448w	γ_{ring}
359s	364s	363s	-	Cr-Cl
331s	342s	339s	340m	Cr-Cl
300s	306s	306s	329m	Cr-Cl
221s	221s	221s	230m 205m	Cr-N(py)

ν = stretching, δ = in plane bending, γ = out of plane bending, vs = very strong, s = strong, m= medium, w = weak, vw = very weak

2.2.3   COMPUTATIONAL STUDY

In order to complement or verify the above vibrational assignments, DFT calculations were carried out on $[CrCl_3(py)_3]$ to allow the generation of the theoretical IR and Raman spectra in the minimised conformation. Comparisons between these and the spectra obtained experimentally showed that the frequencies correlate extremely well. These comparisons are illustrated in Figure 2.8 (MIR) and Figure 2.9 (full Raman). Figure 2.10 highlights the FIR region (but is also the case in the far Raman region) whereby only one Cr–Cl vibration appears to be visible in the calculated spectrum. This is a direct result of the solid state effects which result from the fact that the computed spectrum reflects the vibrations of an isolated gas–phase molecule, thus ignoring any intermediate perturbations. With the aid of computational software, the other Cr–Cl modes were identified.
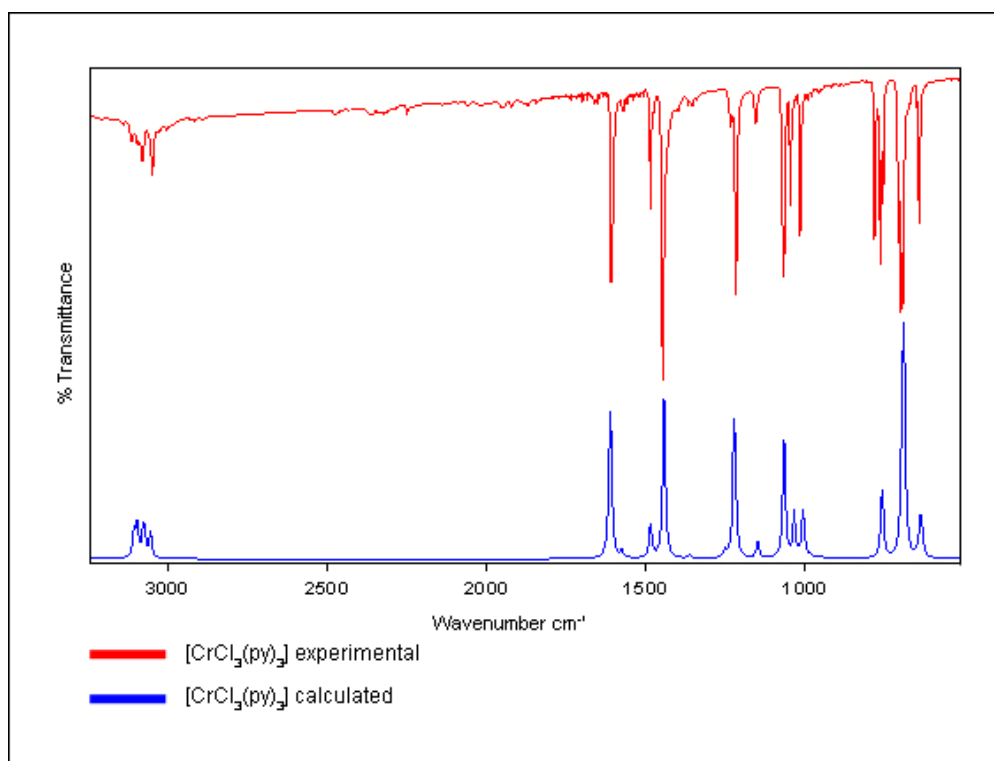
Figure 2.8   **Experimental (red) and calculated (blue) MIR spectra of $[CrCl_3(py)_3]$**
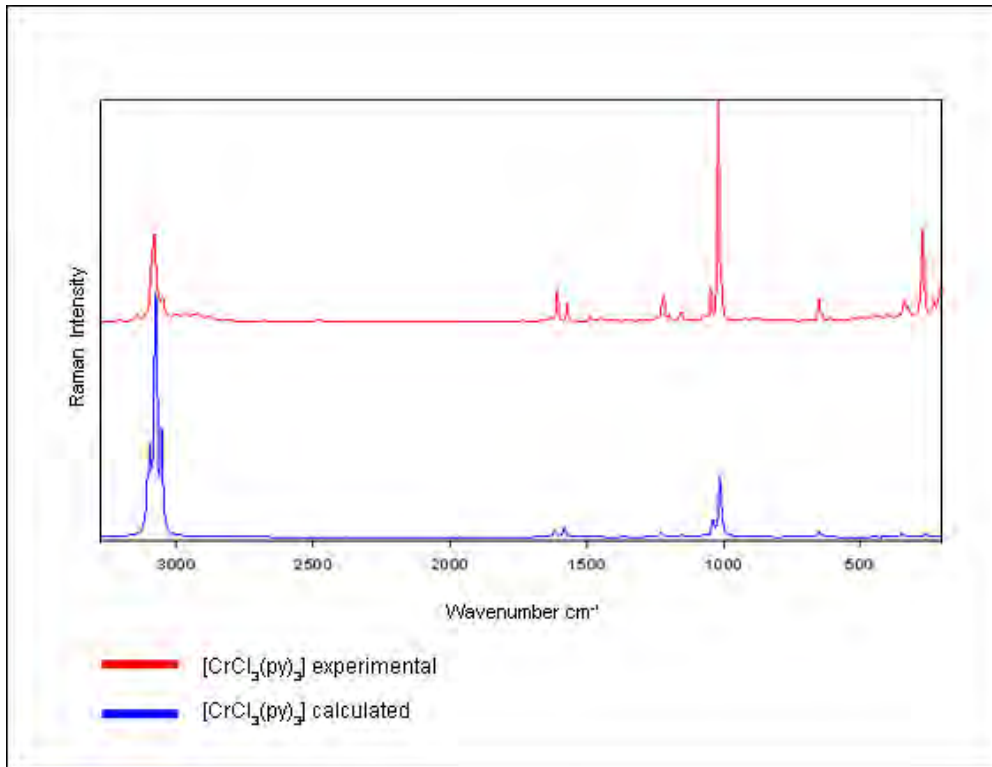
Figure 2.9   **Experimental (red) and calculated (blue) Raman spectra of [CrCl$_3$(py)$_3$]**
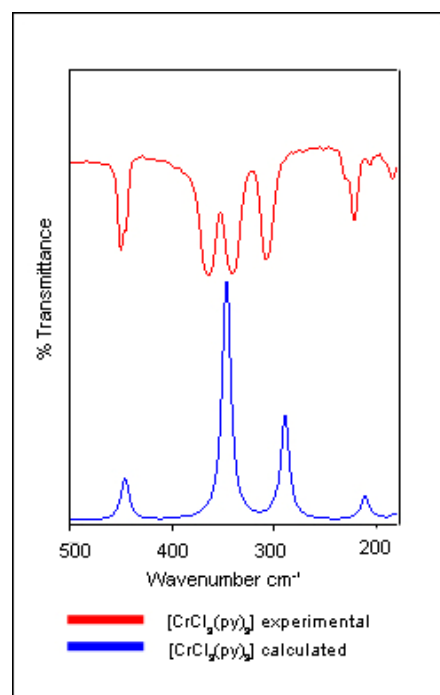
Figure 2.10   **Experimental (red) and calculated (blue) FIR spectra of [CrCl$_3$(py)$_3$]**

Table 2.3 highlights a number of the important vibrations that are indicative of pyridine coordination, which include ring vibrations and metal–ligand vibrations. With regard to the latter, there are some discrepancies with the lower than expected Cr–Cl vibration at 255 cm^{-1} and the higher than expected Cr–N vibration at 290 cm^{-1}. Another observation that is worthy of mention is the absence of the characteristic C–O–C coordinated thf vibration at ~856 cm^{-1} in the calculated IR spectrum. This is thus an indirect reiteration of its assignment. Table 2.4 presents the scaling factors determined for $[CrCl_3(py)_3]$.

Table 2.3   **Selected experimental and calculated IR and Raman band assignments for $[CrCl_3(py)_3]$**

$[CrCl_3(py)_3]$ IR / cm^{-1}		$[CrCl_3(py)_3]$ Raman / cm^{-1}		Assignment	
Experimental	**Calculated**	**Experimental**	**Calculated**	**Experimental**	**Calculated**
1609	1611	1607	1617	ν_{ring}	ν_{ring}
1447	1444	1449	-	ν_{ring}	ν_{ring}
1046	1035	1046	1038	ν_{ring}	ν_{ring}
1014	1006	1018	1014	Ring breathing (py)	Ring breathing (py)
763/754	759	768	761	γ (CH)	γ (CH)
640	638	650/641(sh)	650/640 (sh)	δ_{ring}	δ_{ring}
445	446	448	447	γ_{ring}	γ_{ring}
363, 339, 306	346, 344, 255	340, 329	348, 346, 256	Cr-Cl	Cr-Cl
221	290	230	289	Cr-N	Cr-N

ν = stretching, δ = in plane bending, γ = out of plane bending

Table 2.4   **Scaling factors determined for $[CrCl_3(py)_3]$**

Region / cm^{-1}	IR	Raman
0 – 1854	0.978141	0.974252
2980 – 3434	0.960063	0.960354

In addition to the vibrational data, the HOMO and LUMO orbitals were generated for $[CrCl_3(py)_3]$. From Figure 2.11 it is clear that the chlorine atoms are nucleophilic sites of high electron density which are susceptible to electrophilic attack, while nucleophilic attack will only occur at the pyridine ring system that is *trans* to a chlorine atom. Such electron deficiency is assumed to result from the fact that it is found on a polarisable axis where electrons will be

drawn to the more electronegative chlorine atom. It could also be argued that this high electron density on the chlorine atoms facilitates the formation of bridging chloro ligands for dimeric intermediates.
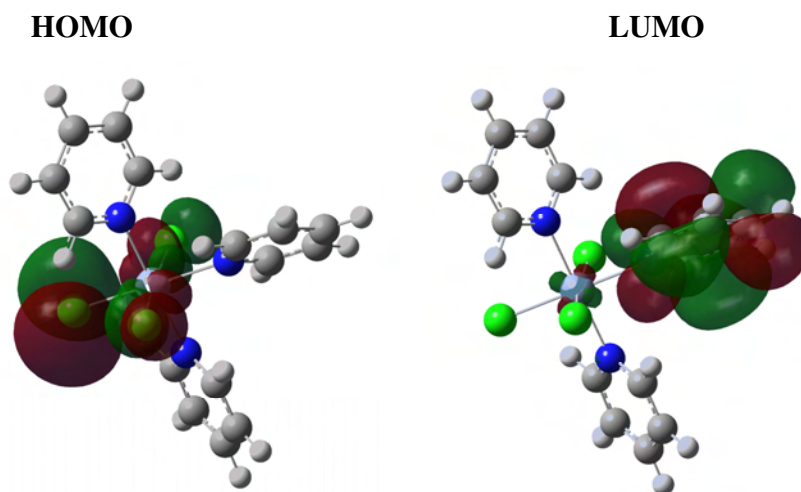
HOMO **LUMO**

**Figure 2.11**   **HOMO and LUMO orbitals of [CrCl$_3$(py)$_3$]**

2.2.4   NMR SPECTROSCOPY

Although this is normally avoided as a plausible means of analysis when investigating paramagnetic Cr(III) metal compounds, a novel ^{1}H NMR experiment was devised which used the paramagnetic effects of the compound as a means of gaining information on ligand coordination and reaction time.

The substitution of thf with three equivalents of pyridine in [CrCl$_3$(thf)$_3$] was followed by proton NMR spectroscopy through slow addition of stoichiometric amounts of pyridine in acetone–d$_6$ to [CrCl$_3$(thf)$_3$] in an NMR tube. Initial attempts to follow the reaction resulted in excessive line broadening and complete loss of the lock signal after *ca.* 10 minutes of the reaction. This problem was solved by adding minimal quantities of the chromium starting material [CrCl$_3$(thf)$_3$], *ca.* 5 mg, and then following the reaction in the spectrometer. Initially at t$_0$ (the start of the experiment), a mixture of thf starting material ($\delta = 1.79–3.63$ ppm) and free, uncoordinated pyridine ($\delta = 7.30–8.57$ ppm) is observed in the spectrum. It must be noted that due to the poor resolution of the spectra, the chemical shift values given are not completely accurate. The coordinated thf ligands in the starting material have resonances that are similar to

those of free thf, which makes differentiation between free and coordinated thf difficult. Due to the ease of obtaining a lock signal for proton NMR spectroscopy using acetone–d$_6$, it was possible to obtain spectra in rapid succession (approximately every four minutes). In so doing the course and progress of the reaction were followed. As the pyridine coordinates to the Cr centre, thus displacing the thf ligands, line broadening is observed in the thf resonance region, while the free pyridine resonances disappear as they coordinate to the chromium centre. After *ca*. 180 minutes the reaction is complete as the free pyridine resonances disappear. This is an important observation because to the naked eye the immediate colour change upon the addition of the three pyridine equivalents initially suggested that the reaction completion time was a matter of minutes, whereas in reality it is ~3 hours.

Figures 2.12 and 2.13 illustrate the similarities in the ^{1}H NMR spectra resonances of both free thf and coordinated thf as observed in the spectrum of the precursor [CrCl$_3$(thf)$_3$].
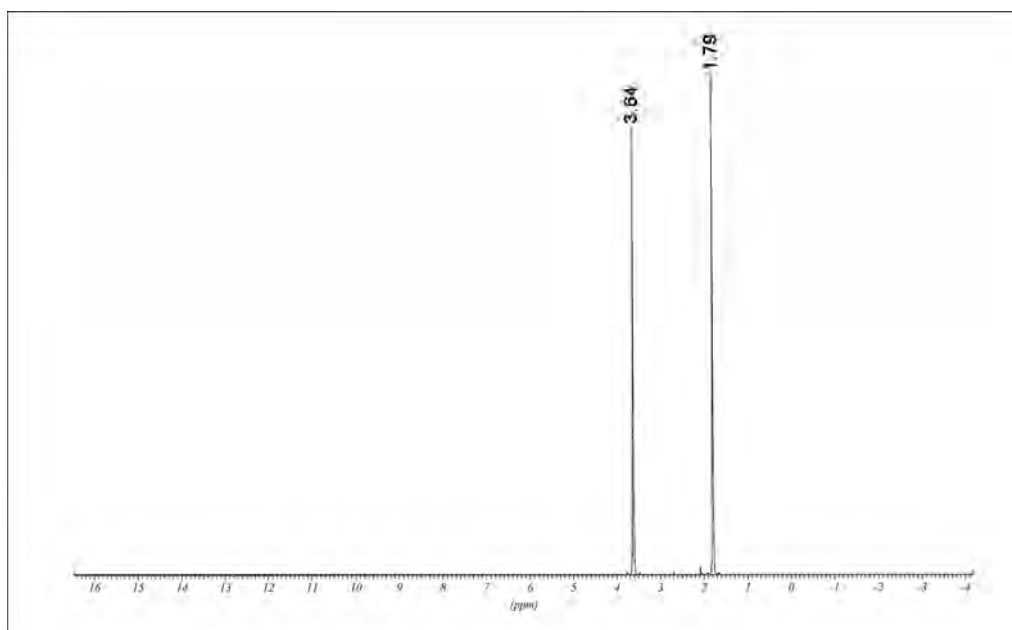
Figure 2.12 ^{1}**H NMR spectrum of free thf in acetone-d$_6$**

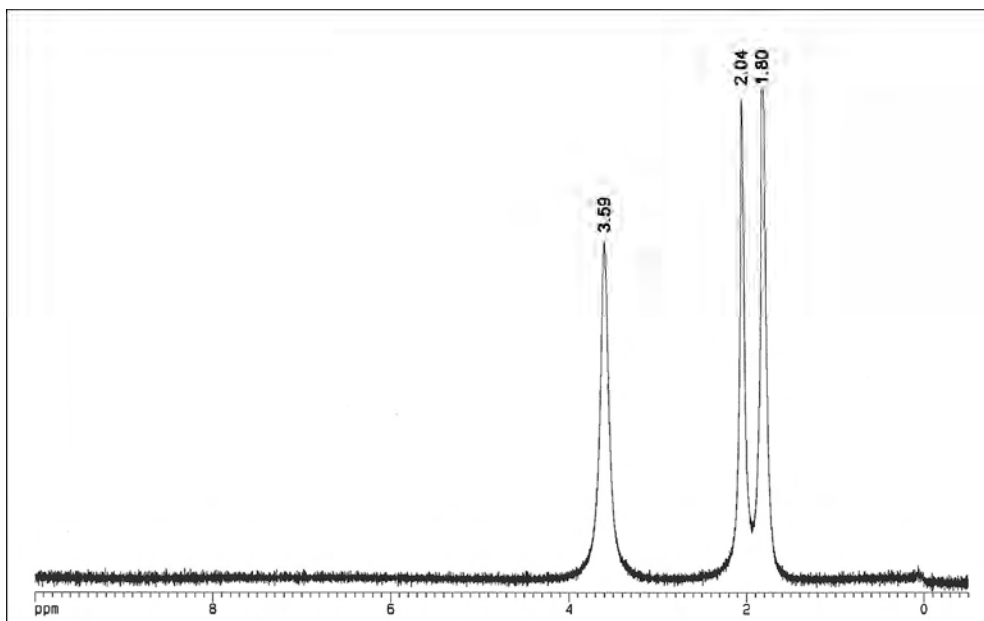**Figure 2.13** ^{1}H NMR spectrum of [CrCl$_3$(thf)$_3$] in acetone-d$_6$

The stacked spectra in Figure 2.14 clearly show how the free pyridine resonances disappear and broaden over time upon coordination to the Cr(III) centre. As expected, there is also an increased amount of free thf (4) as the substitution reaction proceeds.
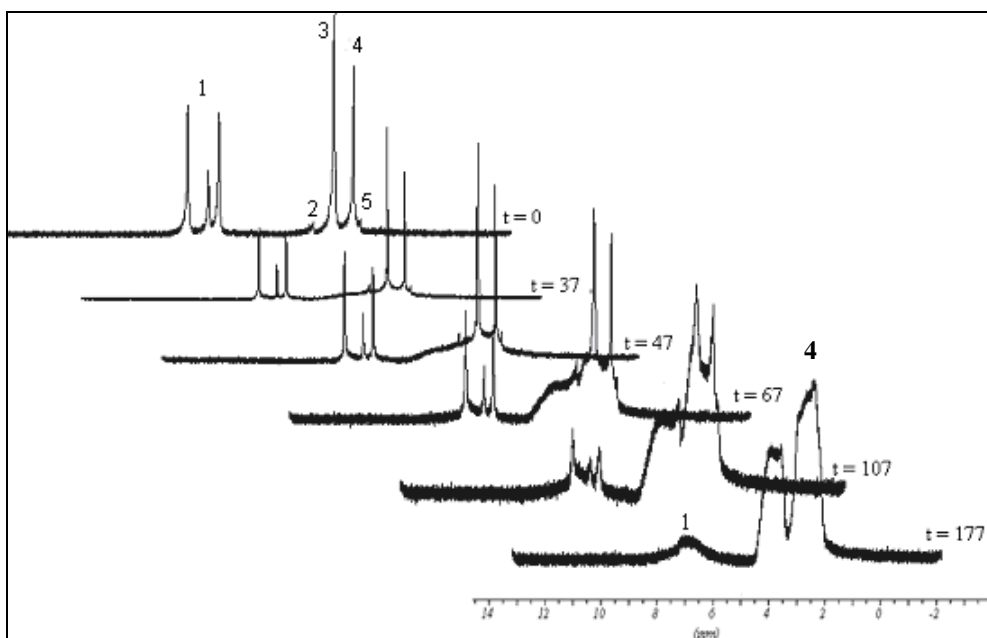

Figure 2.14 Stacked ^{1}H NMR spectra for the reaction of pyridine with [CrCl$_3$(thf)$_3$] over time.
1 = py, 2 = thf, 3 = water peak in acetone, 4 = acetone-d$_6$, 5 = thf

Although one cannot use this data for kinetic investigations (rate determination, etc.), as was mentioned in Chapter 1 it does give valuable insights into the reaction profile and progress.

The sample was left in the instrument and after a further hour had elapsed, another spectrum was recorded. Although the result was the same, the resonance quality of the later spectrum was noticeably higher as can be seen in Figure 2.15.
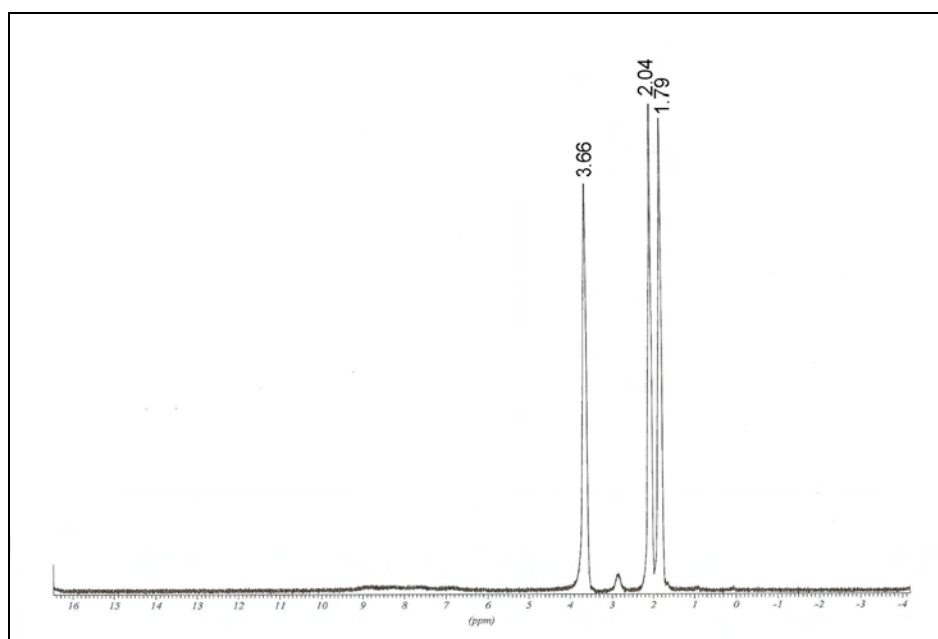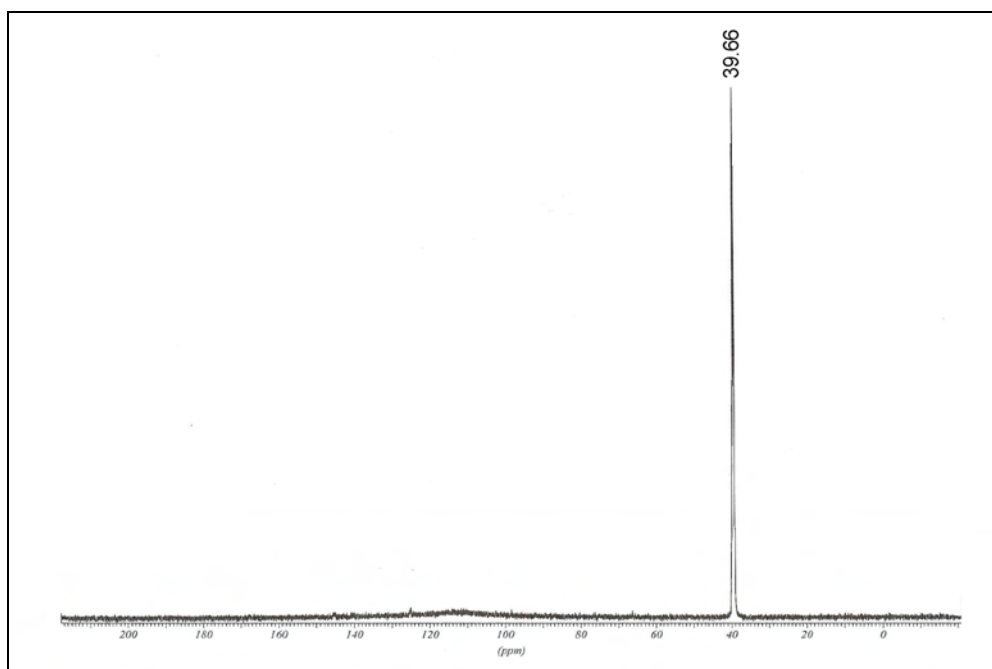

Figure 2.15 ^{1}H NMR spectrum of [CrCl$_3$(py)$_3$] in acetone-d$_6$ after a further hour

Upon removal of the sample from the instrument, a small amount of the expected olive green precipitate was present. This acetone-insoluble product was dried, then dissolved in DMSO–d$_6$ and a subsequent ^{13}C NMR spectrum recorded. As mentioned in the experimental section of Chapter 1, the acetone–d$_6$ and DMSO–d$_6$ spectra are comparable due to no differing solvent-induced shifts and the resulting ^{13}C NMR spectrum.

The absence of any ligand resonances (pyridine and thf) in the resulting ^{13}C NMR spectrum (Figure 2.16) is a notable result for two reasons. Firstly, it is a strong indication of pyridine coordination and secondly, it suggests that the thf resonances observed in the final ^{1}H NMR reaction spectra above are associated with free thf (Figures 2.14 and 2.15).

Figure 2.16 ^{13}C NMR spectrum of [CrCl$_3$(py)$_3$] precipitate formed after removal of above reaction from NMR instrument

2.2.5   X-RAY CRYSTALLOGRAPHY

2.2.5.1   [CrCl$_3$(py)$_3$]

A wide range of solvents and crystallisation techniques were utilised in attempts to obtain and isolate single crystals of these compounds that could be analysed on the single crystal diffractometer. Note that a further hint that [CrCl$_3$(py)$_3$] was formed in all four experiments was given by their similar solubilities. As was stated in Chapter 1, the insoluble nature of these types of compound proved in general to be troublesome.

However, with regard to this category three single crystals of sufficiently good quality were isolated. The first two (crystals of the addition of two and three molar equivalents of pyridine) were grown from CH$_3$CN and, perhaps unsurprisingly, were identical in structure. Along with the visual and IR analysis, this was a further, and in fact stronger, indication of the inability to control the addition of individual monodentate ligands. What is implied is that the addition of one or two pyridine ligands suffices to activate and increase the lability of the remaining thf

40

molecules. From a mechanistic point of view this is an important result as it is an indication that compound formation could take place via direct ligand substitution or indeed via symmetrical cleavage of a dimeric species. Although the structure had previously been determined by Howard [83], structural differences were observed as a result of the encaptured CH_3CN solvent molecule found within the unit cell of this study's structure. Figure 2.17 compares perspective drawings of both the structure determined in this study and that of Howard [83].
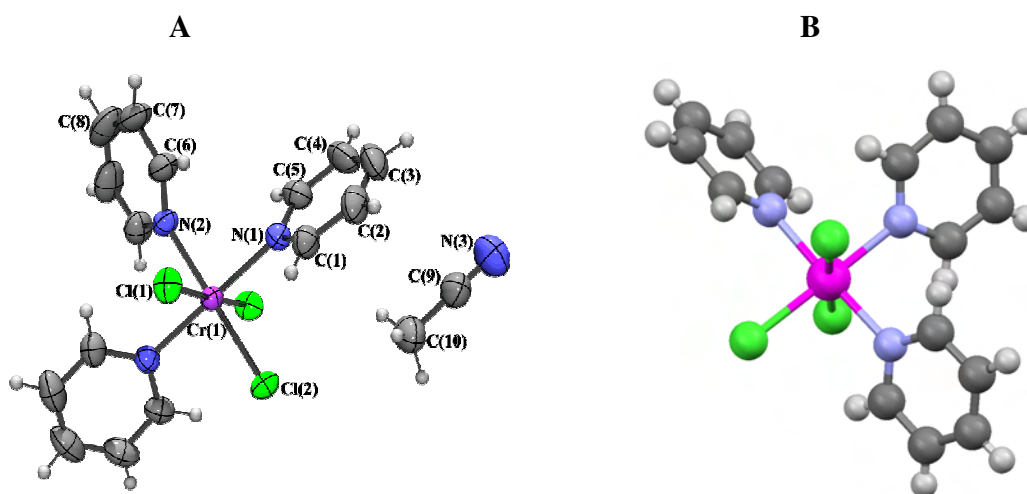
Figure 2.17   **A = Perspective drawing of [CrCl₃(py)₃] structure determined in this study, B = Perspective drawing of [CrCl₃(py)₃] structure determined by Howard [83]**

In both instances, the chromium atom is coordinated to three chlorine atoms and three nitrogen atoms of the individual pyridine molecules in a clear *mer* fashion. The coordination is approximately octahedral, with the Howard structure [83] exhibiting the greatest deviation of 2.14° which relates to the Cl(2)–Cr(1)–Cl(1) angle. The corresponding angle in addition to N(2)–Cr(1)–Cl(1) both exhibit the largest deviation from this study's structure of 1.61°. All the other angles of this structure fall within the range 89.36(4)–90.64(4)°, which is similar to the range of Howard [83] between 88.4(1) and 91.8(1)°.

With regard to bond lengths, the focus has centred on the metal–ligand bonds. As expected, these are virtually identical for both structures as the pyridine ligands are sterically and electronically identical. Table 2.5 highlights these bond lengths and also includes the bond angles that indicate the approximate octahedral geometry.

Table 2.5   **Selected bond lengths [Å] and angles [°] for [CrCl₃(py)₃]**

Cr(1)-N(2)	2.1037(17)	Cr(1)-Cl(2)	2.3196(6)
Cr(1)-N(1)#1	2.1040(13)	Cr(1)-Cl(1)#1	2.3304(4)
Cr(1)-N(1)	2.1040(13)	Cr(1)-Cl(1)	2.3304(4)
N(2)-Cr(1)-N(1)#1	90.06(3)	N(1)-Cr(1)-Cl(1)#1	89.36(4)
N(2)-Cr(1)-N(1)	90.06(3)	Cl(2)-Cr(1)-Cl(1)#1	91.614(11)
N(1)#1-Cr(1)-Cl(2)	89.94(3)	N(2)-Cr(1)-Cl(1)	88.386(11)
N(1)-Cr(1)-Cl(2)	89.94(3)	N(1)#1-Cr(1)-Cl(1)	89.36(4)
N(2)-Cr(1)-Cl(1)#1	88.386(11)	N(1)-Cr(1)-Cl(1)	90.64(4)
N(1)#1-Cr(1)-Cl(1)#1	90.64(4)	Cl(2)-Cr(1)-Cl(1)	91.614(11)

Symmetry transformations used to generate equivalent atoms:
#1 -x,y,-z+1/2

One of the differences between the two structures is seen in the analysis of the torsion angles involving the coordination of the pyridine molecules to the metal centre. Figure 2.18 shows that the pyridine ring systems of the two structures twist in opposite directions to each other relative to one of the axial chlorines. A look at the actual angles reveals notable differences, which indicate that these oppositely twisted rings are not enantiomers of each other. The comparisons of torsion angles in Table 2.6 below are limited to the twisting relative to the axial chlorine atoms.

Table 2.6   **Selected torsion angles [°] for [CrCl₃(py)₃]**

Cl(1)#1-Cr(1)-N(1)-C(1)	-137.42(11)	Cl(1)#1-Cr(1)-N(2)-C(6)	-130.63(9)
Cl(1)-Cr(1)-N(1)-C(1)	45.81(11)	Cl(1)-Cr(1)-N(2)-C(6)	49.37(9)
Cl(1)#1-Cr(1)-N(1)-C(5)	38.36(12)	Cl(1)#1-Cr(1)-N(2)-C(6)#1	49.37(9)
Cl(1)-Cr(1)-N(1)-C(5)	-138.41(12)	Cl(1)-Cr(1)-N(2)-C(6)#1	-130.63(9)

Symmetry transformations used to generate equivalent atoms:
#1 -x,y,-z+1/2
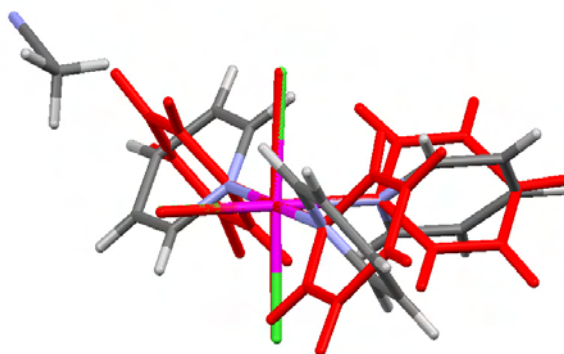
Figure 2.18 **The ring twists observed for [CrCl₃(py)₃] of this study (grey) and that of Howard [83] (red)**

Even though both structures are monoclinic, differences are observed in the crystal data, including the space group, cell dimensions, volume and R–factor.

Table 2.7 **Differences in crystal data between [CrCl₃(py)₃] of this study and that of Howard [83]**

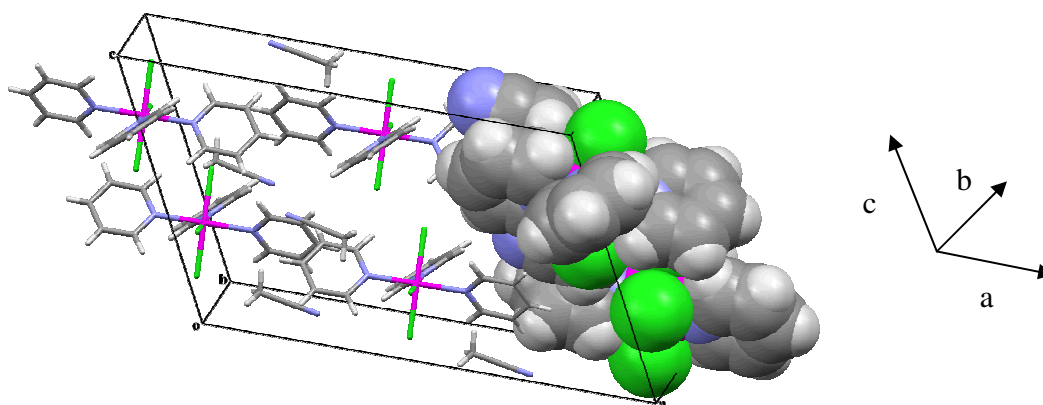| Crystal data	[CrCl₃(py)₃] – This study		[CrCl₃(py)₃] – Howard [83]	
Space group	C 2/c		P 2₁/n	
Cell dimensions	a = 19.3355(12) Å	α = 90°	a = 9.088 Å	α = 90°
	b = 10.8197(7) Å	β = 116.5860(10)°	b = 12.42 Å	β = 91.33°
	c = 11.9758(8) Å	γ = 90°	c = 15.557 Å	γ = 90°
Volume	2 240.5(3) Å³		1 758.598 Å³	
Volume/non-H atoms	20.0 Å³		19.9 Å³	
R-factor	2.99%		5.2%	

More details of the crystal and structure refinement of this study's structure are given in Table 2.7, while a full set of crystallographic tables is to be found in the appendix.

From the differences observed in Table 2.7 above it is the notably lower R–factor for the complex solved in this study that deserves particular mention.

Note that no hydrogen bond interactions were observed between the CH_3CN and the Cr compound, a finding that is reiterated by the very similar volumes/non-hydrogen atoms calculated for both structures. However, within the packing arrangement (Figures 2.19 and 2.20) there are short contacts that may be defined as weak hydrogen bond interactions as they exist between a chlorine atom and the hydrogen of the pyridine ring at distances of 2.948 Å.
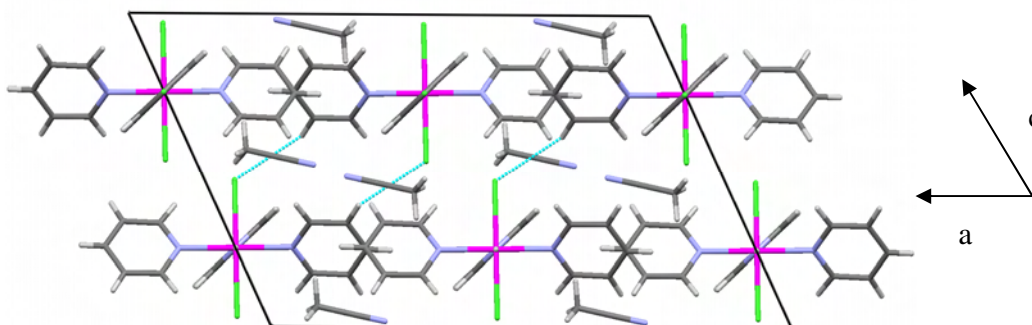
Figure 2.19   **Short contacts observed in the packing arrangement of [CrCl₃(py)₃] of this study**

Figure 2.20   **Packing arrangement of [CrCl₃(py)₃] of this study which includes space fill arrangement**

The crystal data and structure refinement for [CrCl$_3$(py)$_3$] is presented in Table 2.8.

Table 2.8   **Crystal data and structure refinement for [CrCl₃(py)₃] of this study**

_____

Empirical formula	$C_{19} H_{21} Cl_3 Cr N_5$
Formula weight	477.76
Temperature	293(2) K
Wavelength	0.71073 Å
Crystal system	Monoclinic
Space group	C 2/c
Unit cell dimensions	a = 19.3355(12) Å $\alpha = 90°$
	b = 10.8197(7) Å $\beta = 116.5860(10)°$
	c = 11.9758(8) Å $\gamma = 90°$

Volume	2 240.5(3) Å^3
Z	4
Density (calculated)	1.416 Mg/m^3
Absorption coefficient	0.883 mm^{-1}
F(000)	980
Crystal size	0.42 x 0.24 x 0.22 mm^3
Theta range for data collection	3.25 to 26.48°
Index ranges	-22<=h<=19, -13<=k<=8, -9<=l<=14
Reflections collected	5 912
Independent reflections	2 128 [R(int) = 0.0237]
Completeness to theta = 25.00°	99.5%
Absorption correction	Semi-empirical from equivalents
Max. and min. transmission	0.823 and 0.681
Refinement method	Full-matrix least-squares on F^2
Data / restraints / parameters	2 128 / 0 / 171
Goodness-of-fit on F^2	1.059
Final R indices [I>2σ(I)]	R1 = 0.0299, wR2 = 0.0828
R indices (all data)	R1 = 0.0323, wR2 = 0.0860
Extinction coefficient	0
Largest diff. peak and hole	0.281 and -0.251 e.Å^{-3}

_____

2.2.5.2   [Hpy][CrCl₄(py)₂] (4)

The second structure was unexpected and most interesting in nature as it posed questions regarding the synthetic pathway via which compounds of this nature form. The light green diamond-shaped crystals were grown from the NMR solution of $[CrCl_3(thf)_3]$ and three pyridine equivalents in acetone–d_6 that had been used in the above NMR study. The growth period was five days.

This anionic chromium species with a cationic counter-ion has in fact been synthesised previously but, importantly, no crystal structure was ever obtained.

One of the first mentions of $[Hpy][CrCl_4(py)_2]$ in the literature was in 1973 when Brown and Richardson carried out thermal decomposition studies on it and related Cr(III) compounds, including $[CrCl_3(py)_3]$ [41]. It should be noted that the synthetic route to produce $[Hpy][CrCl_4(py)_2]$ was a most awkward procedure which involved $[CrCl_3.6H_2O]$, pyridine, thionyl chloride and benzene. Their analysis led them to the conclusion that $[CrCl_3(py)_3]$ decomposes upon heating to give the dimeric species $[Cr_2Cl_6(py)_4]$, while the thermal decomposition of $[Hpy][CrCl_4(py)_2]$ led to the same dimer via the loss of pyHCl [41].

Interest in $[Hpy][CrCl_4(py)_2]$ resurfaced again in 1990 when Brenčič [84] were able to remake the compound via a simpler and more straightforward method involving the addition of pyHCl to $[CrCl_3(py)_3]$. Their particular interest lay not in any mechanistic details but in the adopted configuration of the $[Hpy][CrCl_4(py)_2]$ compound. In addition to evidence from other similar compounds, they concluded that it adopts the *trans* configuration due largely to the fact that when pyridine is added to $[Hpy][CrCl_4(py)_2]$, the trans $[CrCl_3(py)_3]$ forms.

1. $[CrCl_3(py)_3] + pyHCl \longrightarrow [Hpy][CrCl_4(py)_2] + py$

2. $[Hpy][CrCl_4(py)_2] \longrightarrow [CrCl_3(py)_3] + HCl$
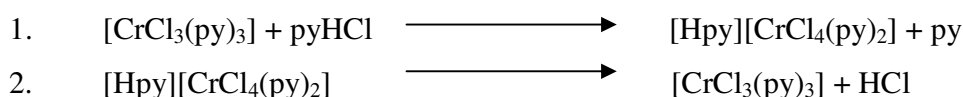
The determination of this crystal as part of this study was able to confirm Brenčič's predictions of *trans* conformer formation. Also, more weight was added to the dimeric link proposed by Brown and Richardson [41] as in relation to this study $[Hpy][CrCl_4(py)_2]$ had to have formed from an asymmetrically cleaved dimeric intermediate. This correlates well with the grey/blue intermediatory colour seen in these compounds that Elowe [38] associated with dimeric species, as mentioned earlier. Thus, what is implied is that perhaps more than one mechanism is plausible. The first is direct ligand substitution as suggested previously. However, in the light of this anionic chromium-type structure, one must certainly entertain the possibility of dimer formation.

This can be cleaved either symmetrically or asymmetrically, resulting in the neutral monomer or the anionic chromium species [Hpy][CrCl$_4$(py)$_2$] incorporating the pyridinium counter-ion. The asymmetrical cleavage would also have resulted in the other portion of the dimer, which would possess a cationic chromium species. Interestingly with regard to previous studies in this field, it is the cationic chromium species that is assigned as the catalytically active species, as mentioned in Chapter 1. It was unfortunate that this species could not be isolated. The possible pathways to product formation are presented in Figure 2.21.
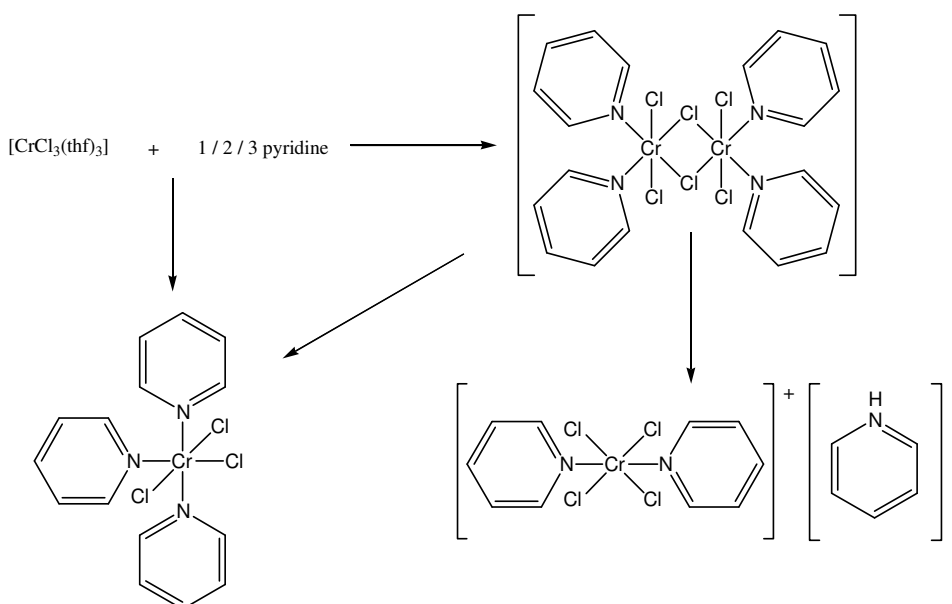
Figure 2.21   **Possible pathways to product formation**

The next logical question concerns the driving force behind symmetrical and asymmetrical cleavage. The only difference in how the [CrCl$_3$(py)$_3$] and [Hpy][CrCl$_4$(py)$_2$] compounds were formed was that their solvents of crystallisation differed ([CrCl$_3$(py)$_3$] = CH$_3$CN, [Hpy][CrCl$_4$(py)$_2$] = acetone–d$_6$).

Of the limited number of CrCl$_4$L$_2$ (L = donor ligands) crystal structures that have been solved throughout the literature, only two structures (excluding the structure [Hpy][CrCl$_4$(py)$_2$]) possess unlinked monodentate donor ligands that are coordinated to the chromium centre via single bonds. They are:

- Trimethylphosphoniumtrans–tetrachloro–bis–(trimethylphosphine)– chromium(III) [85].

- Quinolinium tetrachloro–bis(acetonitrile) chromium (III) acetonitrile solvate [86].

Of these two, 3D coordinates were available only for the former. In this novel [Hpy][CrCl$_4$(py)$_2$] compound the chromium atom is coordinated to four chlorine atoms and two nitrogen atoms of the pyridine ligands, while that in literature has the chromium atom coordinated to four chlorine atoms and two trimethylphosphine ligands. In both cases similar donor ligands are *trans* to each other. The coordination of this novel pyridine-based compound is approximately octahedral with the largest deviation being the Cl(3)–Cr(1)–Cl(4) bond angle (88.28(3))°. All other *cis* X–Cr–Y bond angles are in the range 89.17(7) to 91.12(3)°. The metal–ligand bond lengths were, unsurprisingly, of very similar magnitudes to those of [CrCl$_3$(py)$_3$].

The torsion angles for both pyridine ligands are virtually identical (difference of 1.5° between C(1)–N(1)–Cr(1)–Cl(1) and C(10)–N(2)–Cr(1)–Cl(1)) as they are observed in the same plane. This aromatic planarity is presented in Figure 2.22. The observed tilting of the pyridinium ion is discussed under the paragraph that highlights hydrogen bonding.
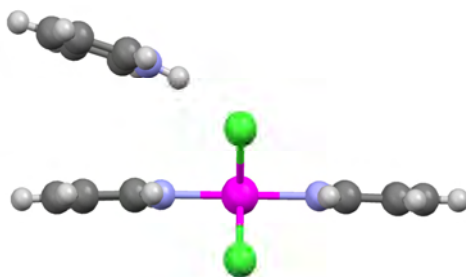
Figure 2.22 **The planarity of the pyridine rings as well as the tilting of the pyridinium ion**

Table 2.9 presents a combination of metal–ligand bond lengths, bond angles associated with the octahedral geometry and torsion angles relative to the axial chlorine atoms.

Unlike the phosphine-based structure in the literature, hydrogen bonding is observed between the pyridinium cation and the anionic chromium species. The pyridinium N(3)–H(3N) group is hydrogen bonded to Cl(3) and Cl(4). A consequence of these interactions is the tilting of the pyridinium ion towards the respective chlorine atoms. This phenomenon can be seen clearly in both Figures 2.22 and 2.23, while Table 2.10 details the interactions.

Table 2.9   **Selected bond lengths [Å], bond angles [°] and torsion angles [°] for [Hpy][CrCl₄(py)₂]**

|			
Cr(1)-N(1)	2.097(2)	Cr(1)-Cl(1)	2.3398(8)
Cr(1)-N(2)	2.109(2)	Cr(1)-Cl(3)	2.3451(8)
Cr(1)-Cl(2)	2.3387(8)	Cr(1)-Cl(4)	2.3490(8)
N(1)-Cr(1)-Cl(2)	90.36(6)	N(2)-Cr(1)-Cl(3)	90.41(7)
N(2)-Cr(1)-Cl(2)	89.95(6)	Cl(2)-Cr(1)-Cl(3)	91.12(3)
N(1)-Cr(1)-Cl(1)	90.43(6)	N(1)-Cr(1)-Cl(4)	90.23(6)
N(2)-Cr(1)-Cl(1)	89.17(7)	N(2)-Cr(1)-Cl(4)	89.46(6)
Cl(2)-Cr(1)-Cl(1)	90.05(3)	Cl(1)-Cr(1)-Cl(4)	90.54(3)
N(1)-Cr(1)-Cl(3)	89.99(6)	Cl(3)-Cr(1)-Cl(4)	88.28(3)
Cl(2)-Cr(1)-N(1)-C(1)	-133.5(2)	Cl(2)-Cr(1)-N(2)-C(10)	135.0(2)
Cl(1)-Cr(1)-N(1)-C(1)	-43.4(2)	Cl(1)-Cr(1)-N(2)-C(10)	44.9(2)
Cl(3)-Cr(1)-N(1)-C(1)	135.4(2)	Cl(3)-Cr(1)-N(2)-C(10)	-133.9(2)
Cl(4)-Cr(1)-N(1)-C(1)	47.1(2)	Cl(4)-Cr(1)-N(2)-C(10)	-45.6(2)
Cl(2)-Cr(1)-N(1)-C(5)	44.9(2)	Cl(2)-Cr(1)-N(2)-C(6)	-43.4(2)
Cl(1)-Cr(1)-N(1)-C(5)	134.9(2)	Cl(1)-Cr(1)-N(2)-C(6)	-133.5(2)
Cl(3)-Cr(1)-N(1)-C(5)	-46.3(2)	Cl(3)-Cr(1)-N(2)-C(6)	47.7(2)
Cl(4)-Cr(1)-N(1)-C(5)	-134.5(2)	Cl(4)-Cr(1)-N(2)-C(6)	136.0(2)

Table 2.10   **Hydrogen bonds for [Hpy][CrCl₄(py)₂] [Å and °]**

D-H...A	d(D-H)	d(H...A)	d(D...A)	<(DHA)
N(3)-H(3N)...Cl(4)	0.89(5)	2.43(5)	3.235(4)	150(5)
N(3)-H(3N)...Cl(3)	0.89(5)	2.94(5)	3.586(4)	131(4)
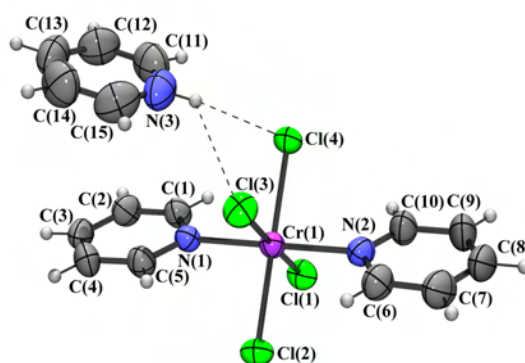
Figure 2.23   **Hydrogen bonding observed in [Hpy][CrCl₄(py)₂]**

Figures 2.24 to 2.27 illustrate the packing arrangement and space filling adopted by the structure with no short contacts of importance visible between the layers.
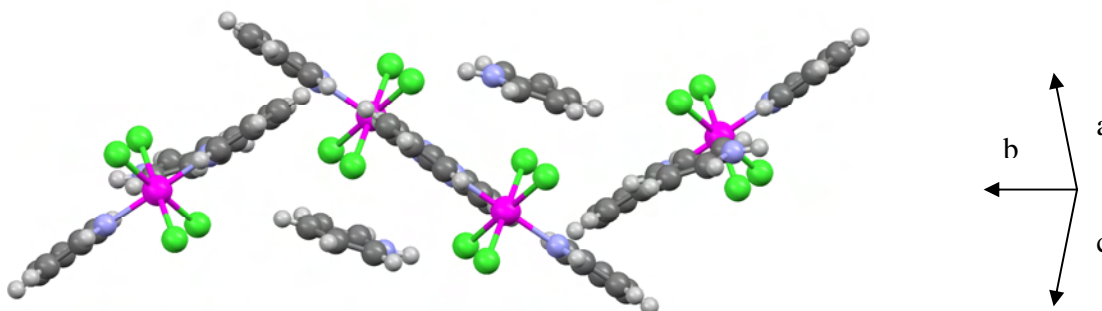
Figure 2.24   **Packing arrangement of [Hpy][CrCl₄(py)₂]**

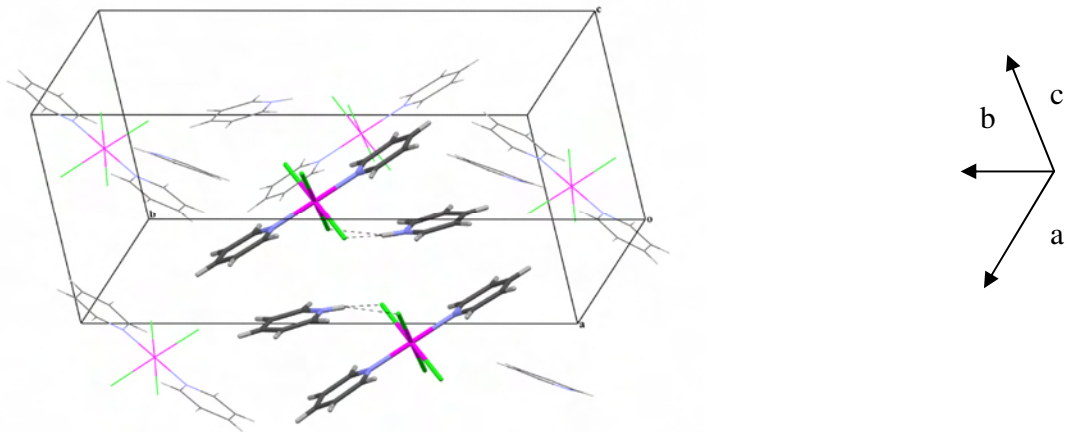**Figure 2.25**   Alternative view of the packing arrangement of [Hpy][CrCl$_4$(py)$_2$]

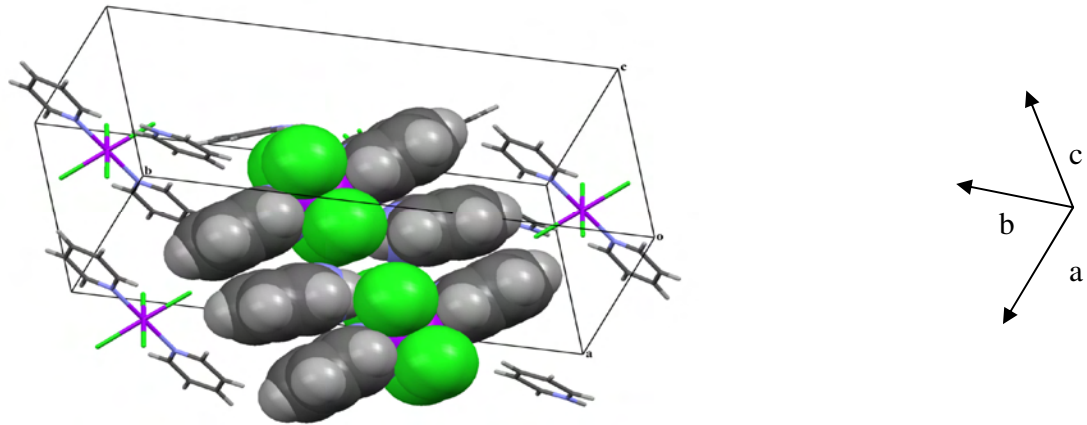**Figure 2.26**   Packing and space fill of [Hpy][CrCl$_4$(py)$_2$]

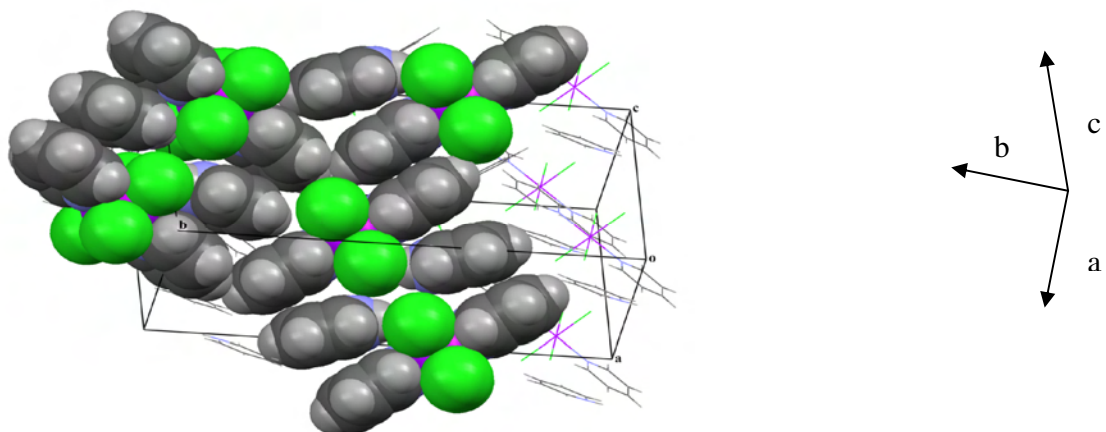**Figure 2.27**   Alternative view of the packing and space fill of [Hpy][CrCl$_4$(py)$_2$]

Crystal data and details of structure refinement are shown in Table 2.11, while the complete set of crystallographic data is given in the appendix.

Table 2.11   Crystal data and structure refinement for [Hpy][CrCl$_4$(py)$_2$]

_____

Empirical formula	$C_{15} H_{16} Cl_4 Cr N_3$
Formula weight	432.11
Temperature	298(2) K
Wavelength	0.71073 Å
Crystal system	Monoclinic
Space group	P 2$_1$/n
Unit cell dimensions	a = 8.1070(7) Å $\alpha = 90°$
	b = 22.5413(18) Å $\beta = 92.9970(10)°$
	c = 10.1760(8) Å $\gamma = 90°$
Volume	1857.0(3) Å^3
Z	4
Density (calculated)	1.546 Mg/m^3
Absorption coefficient	1.192 mm^{-1}
F(000)	876
Crystal size	0.22 x 0.14 x 0.12 mm^3
Theta range for data collection	2.67 to 26.51°.
Index ranges	-10<=h<=10, -12<=k<=28, -10<=l<=12
Reflections collected	10 038
Independent reflections	3 531 [R(int) = 0.0345]
Completeness to theta = 25.00°	99.7%
Absorption correction	Semi-empirical from equivalents
Max. and min. transmission	0.867 and 0.724
Refinement method	Full-matrix least-squares on F^2
Data / restraints / parameters	3 531 / 0 / 211
Goodness-of-fit on F^2	1.087
Final R indices [I>2sigma(I)]	R1 = 0.0351, wR2 = 0.0828

R indices (all data)	R1 = 0.0538, wR2 = 0.0950
Extinction coefficient	0
Largest diff. peak and hole	0.344 and -0.257 e.Å^{-3}

_____

2.2.6   MASS SPECTROMETRY

The FAB-MS spectrum of the [CrCl$_3$(py)$_3$] precipitate shows the isotopic distribution pattern associated with [M–HCl]$^+$ (m/z = 358). This assignment is possible because a crystal structure determination excluded the formation of the dimeric structure, [(μ-Cl)$_2$\{CrCl$_2$(py)$_3$\}$_2$], in the solid state. This pattern correlates strongly with the expected pattern generated by the isotopic distribution calculator. As the [M–3Cl]$^+$ peak (m/z = 289) is also observed it is evident that the chlorine atoms are more readily removed than the pyridine ligands. These findings which are presented in Figure 2.28 verify the already discussed spectroscopic and crystallographic data and provide further evidence that the single crystal determination of [CrCl$_3$(py)$_3$] represents the bulk material.
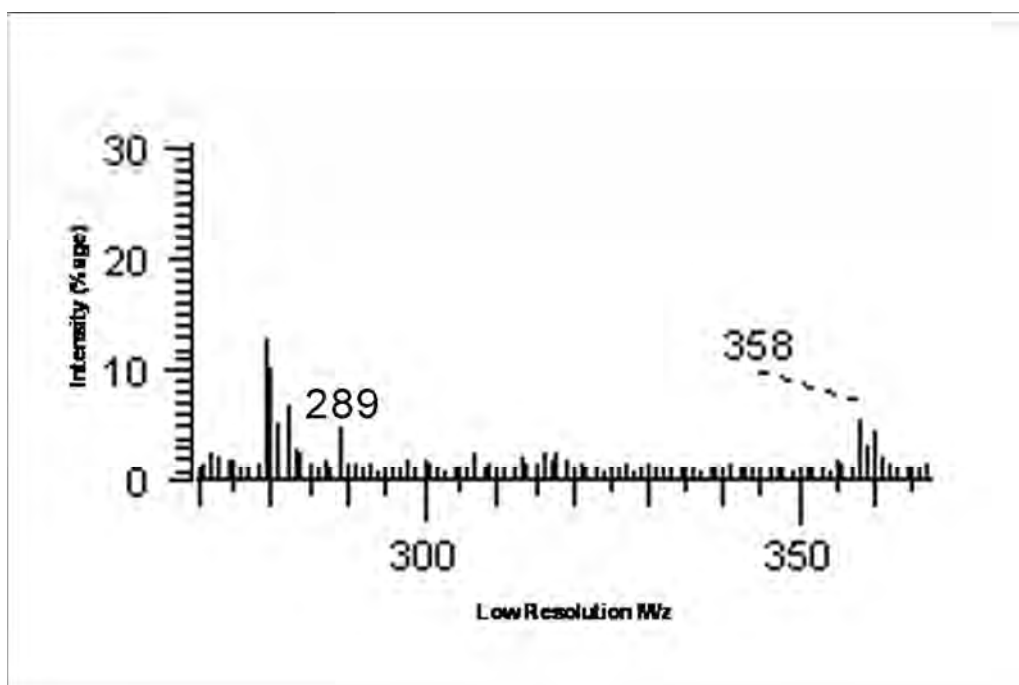


Figure 2.28   FAB-MS spectrum of [CrCl$_3$(py)$_3$]

53

2.3 CATEGORY TWO: BULKY SUBSTITUENTS

One is always aware of selecting ligands that are sterically capable of coordination to the metal centre as bulkiness at a particular position of the ligand may prohibit such coordination. With respect to the addition of pyridines to $[CrCl_3(thf)_3]$, the following question was posed: Would substituents at the ortho position of pyridine prohibit coordination or could the ligands in fact orientate themselves in such a way as to allow coordination to take place? Two reactions were carried out simultaneously (Figure 2.29).

In the first reaction three equivalents of 2,6-dibromopyridine were added to $[CrCl_3(thf)_3]$ in thf, with the interest lying in whether or not the large bromine substituents would allow the endocyclic nitrogen donor atoms of the pyridines to coordinate to the chromium. On immediate addition of the ligand no reaction was visible as the deep colour of $[CrCl_3(thf)_3]$ dissolved in thf remained unchanged. The reaction was then stirred at room temperature and closely monitored. After 12 hours the reaction was stopped as no reaction had yet occurred. The solution was then refluxed at 80°C for a further 12 hours with no change evident.

In the second reaction, to one equivalent of $[CrCl_3(thf)_3]$ was added one molar equivalents of 2,6–dibromopyridine, 2,6–dimethylpyridine and unsubstituted pyridine. All three ligands were added simultaneously to ensure equal competition for sites.

The resulting green precipitate was sparingly soluble in most solvents but dissolved particularly well in DMF. This solution was placed in a fridge and left to crystallise. After a period of four weeks dark green plate-like crystals formed, which were large enough and of sufficiently good quality for analysis on the single crystal diffractometer. The resulting structure was somewhat surprising. All three thf molecules of the chromium precursor had been displaced, but by two equivalents of pyridine and one DMF solvent molecule which had coordinated through the oxygen atom.
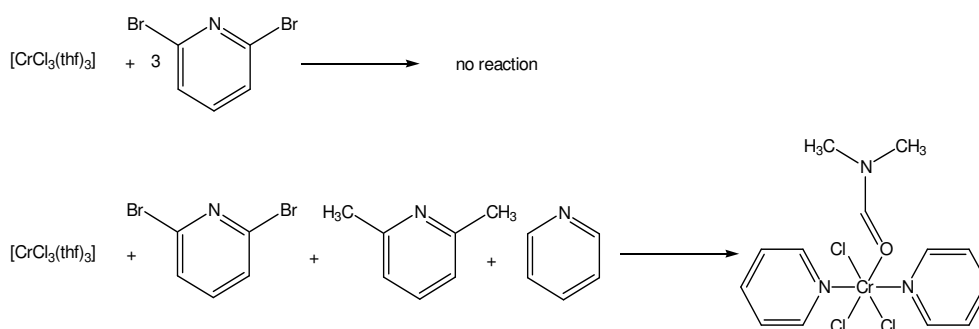
Figure 2.29   Bulky substituent reactions that were carried out

This meant that the question concerning the coordination of ortho substituted pyridines was answered conclusively in the negative. Furthermore, the fact that although only one equivalent of pyridine was added, two such molecules coordinated to the metal centre added weight to the idea discussed in the previous section that only one pyridine would suffice to activate the other available sites. However, with this in mind one would have expected all three available thf sites to have been substituted by pyridines. Instead one of the sites was occupied by a DMF molecule. This is of interest because as a result of the relatively low concentration of pyridine and the labilisation of the thf ligands, one may have expected the formation of a chloro-bridged dimer, which was not observed. It was therefore perceived that DMF was a very good ligand under these conditions.

This finding is yet more evidence supporting the plausibility of direct ligand substitution as a synthetic pathway to compound formation.

As a direct consequence of this resulting structure, it seemed logical to attempt a further reaction whereby all three thf molecules of the precursor could potentially be displaced by three equivalents of the coordinating DMF molecule, thus resulting in a novel structure determination. The reaction involved using DMF as both solvent and ligand. This excess also gave the best possible chance for the DMF to coordinate at the three available sites. On immediate addition of excess DMF to [CrCl$_3$(thf)$_3$] a dark green supernatant was observed. The reaction was stirred overnight at room temperature. In order to mimic the conditions that allowed the formation of [CrCl$_3$(py)$_2$(DMF)] **(5),** the solution was then placed in a fridge. Unfortunately, no crystals were ever formed and

because of the nature of this particular solvent it was not ideal to take the reaction further by reducing the solvent and trying to force out a precipitate. Hence no further attempts were made with regard to this reaction.

2.3.1 INFRARED SPECTROSCOPY

The yield of crystals grown was sufficient for an IR spectrum to be run, but not for the corresponding Raman spectrum. Nonetheless, the IR spectrum was important as the resulting bands could be used as a reference for comparison with those IR spectra of similar compounds where crystals were unobtainable.

Relatively straightforward assignment of bands is possible as the two ligand environments (pyridine and DMF) are very different and thus immune to band overlap.

This result actually serves to reaffirm the conclusion drawn regarding the sequential addition (control of ligand addition) of ligands to [CrCl$_3$(thf)$_3$] – it is not possible via this route.

2.3.1.1 Region 3114–2804 cm^{-1}

This region plays host to three different C–H environments, which include the aromatic heterocycle of pyridine and the methyl and carbonyl functionalities of DMF.

Between 3114 and 3032 cm^{-1} are those vibrations associated with pyridine and they are unshifted relative to the free ligand position, as expected [73, 74, 76]. The methyl frequencies are visible at 3000 and 2940 cm^{-1}, while the carbonyl-specific vibrations are in among them at 2877 and 2804 cm^{-1}[87]. Figure 2.30 highlights these vibrations.
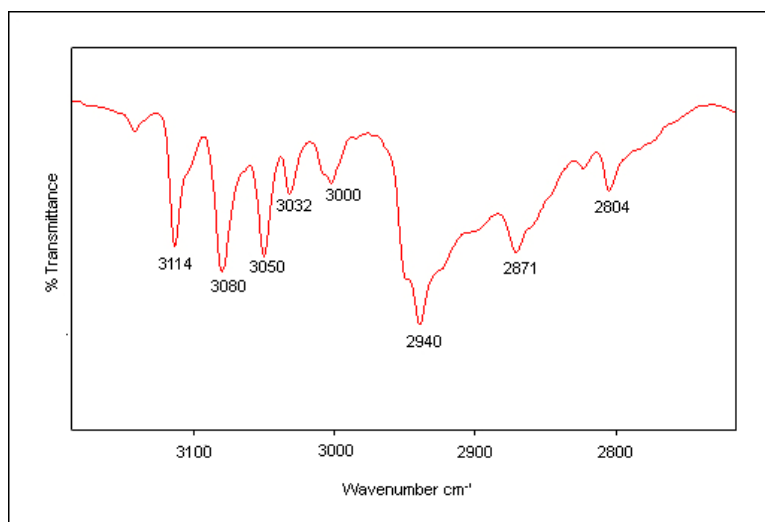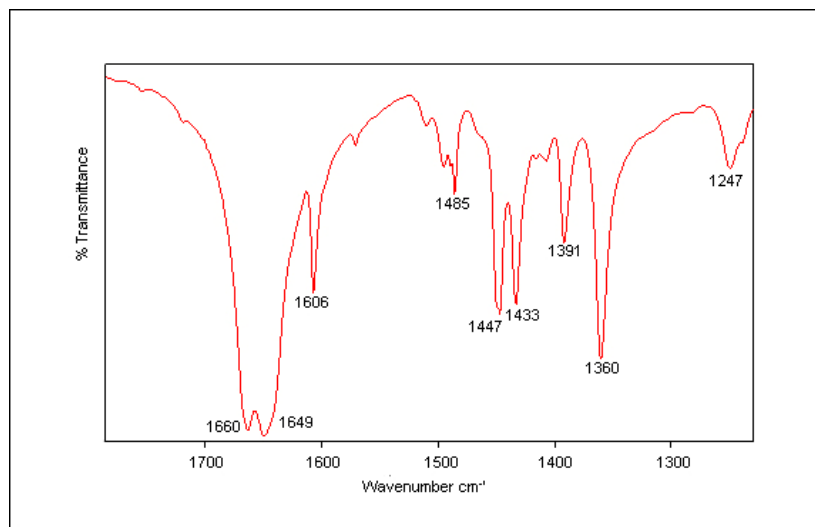
Figure 2.30 **IR spectrum of the region 3114 – 2804 cm^{-1}**

2.3.1.2 Region 1660–1247 cm^{-1}

An informative region with characteristic ligand vibrations is found between 1660–1247 cm^{-1} (see Figure 2.31). The strongest and probably most recognisable vibrations of the entire spectrum are the two vibrations at 1660 and 1649 cm^{-1} which are characteristic of C=O carbonyl stretches of DMF [88]. A band found very close to these modes is the expected pyridine vibration at 1606 cm^{-1} which has shifted from either 1599 cm^{-1} or 1580 cm^{-1} upon coordination [73, 74]. Other pyridine-assignable bands are those at 1572, 1485 and 1446 cm^{-1}, with only that at 1446 cm^{-1} shifting upon coordination from a free pyridine ring vibration of 1438 cm^{-1} [73, 74]. The remaining bands relate to DMF [87] and include:

1433 cm^{-1}	δ(sym) CH$_3$
1391 cm^{-1}	δ N–C–H in plane carbonyl
1247 cm^{-1}	ν(asym) C–N of N(CH$_3$)$_2$

(δ(sym) = symmetrical bending, ν(asym) = asymmetrical stretching)

Figure 2.31 **IR spectrum of the region 1660 – 1247 cm^{-1}**

2.3.1.3 Region 1219– 448 cm^{-1}

Very few bands corresponding to the DMF molecule are found in this region with only that at 1095 cm^{-1} being assignable solely to DMF with any level of surety [89].

The remaining bands are pyridine vibrations, three of which exhibit characteristic shifts indicative of coordination. They are found at 1015, 644 and 448 cm^{-1} and have shifted from their free ligand positions of 991, 605 and 405 cm^{-1} respectively. All three shifts are in accordance with those observed for [CrCl$_3$(py)$_3$] [73, 74]. All important vibrations are presented in Figure 2.32.
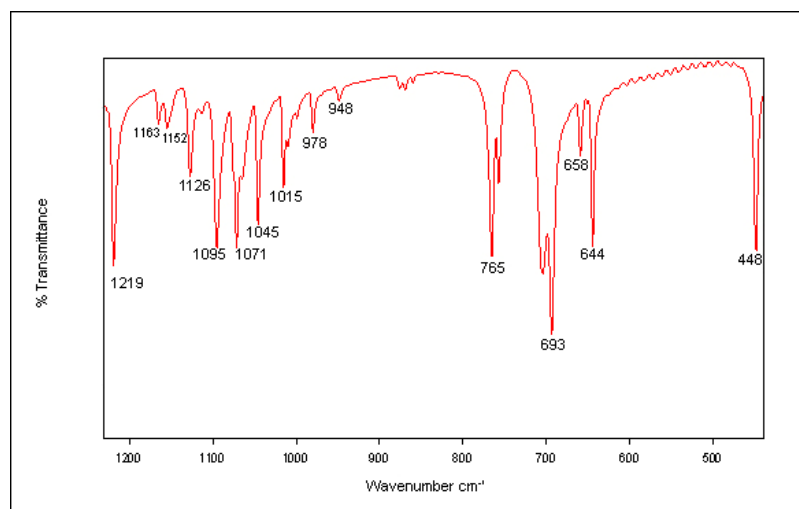
Figure 2.32   IR spectrum of the region 1219 – 448 cm^{-1}

2.3.1.4   Region 415–214 cm^{-1}

More evidence of pyridine coordination by way of characteristic shifts is observed with the vibrations at 644 and 448 cm^{-1}. Their shifting from the free ligand positions of 605 and 405 cm^{-1} is widely accepted [73, 74].

DMF vibrations in the form of C–N–C deformations are also observed at 397 and 390 cm^{-1} [90, 91], although they do overlap with the assignment of a tertiary butyl C–C–C deformation [92].

Relatively distinguishable are the expected three Cr–Cl bands at 358, 324 and 302 cm^{-1} and they are in accordance with the observed *mer* orientation witnessed in the crystal structure [80].

Although the literature asserts that the Cr–N of pyridine band is at 221 cm^{-1} [41, 80, 81], it is plausible that because of its novel ligand environment (the proximity of coordinated DMF), it is now present at 214 cm^{-1}. This then allows for the Cr–O of DMF vibration to be the band at 230 cm^{-1}. It is, however, assigned with a certain amount of caution due to the lack of evidence in the literature.

The IR bands have been tabulated alongside the substituted pyridine compounds which are discussed in the following section due to the coordination of pyridine derivatives in all. Figure 2.33 highlights the vibrations found in this region.
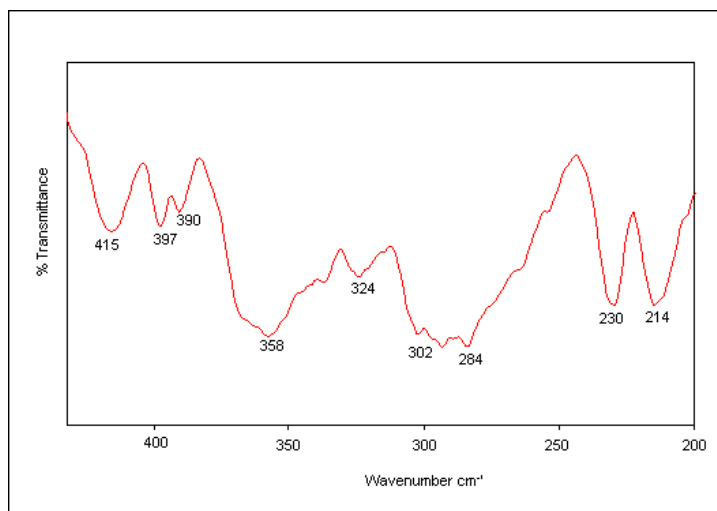

Figure 2.33   **IR spectrum of the region 415 – 214 cm^{-1}**

2.3.2   X-RAY CRYSTALLOGRAPHY

In 1977 Broomhead [88] solved the crystal structure for the compound *mer*-trichloro(dimethylformamide)(1, 10-phenanthroline)chromium(III) which, until the results of this study, was the only known structure of a chromium–DMF complex. Interesting comparisons can be drawn between the two structures although differences are certainly expected as [CrCl$_3$(py)$_2$(DMF)] is essentially the first structure determination in which the nitrogen donor ligands are of a monodentate nature. Figure 2.34 shows the two structures.

In [CrCl$_3$(py)$_2$(DMF)] the central chromium atom is coordinated to three chlorine atoms, two nitrogen atoms of pyridine molecules and an oxygen atom of a DMF molecule. The pyridine ligands are *trans* to each other and unlike the 'Broomhead structure' the DMF is *trans* to a chlorine atom. The coordination is approximately octahedral with the largest deviation being the N(1)–Cr(1)–O(1) bond angle (86.98(10)°). All the other *cis* X–Cr–Y bond angles are in the range 87.90(7)–92.93(7)°.

A   B
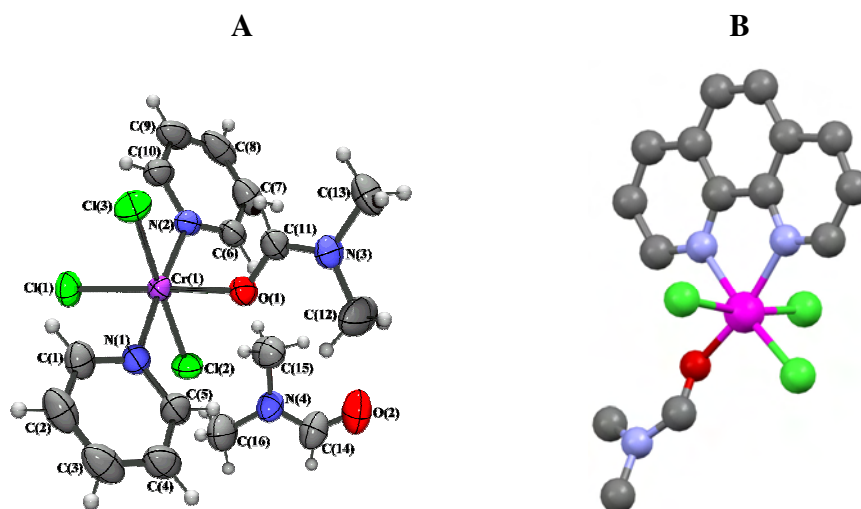
Figure 2.34   **A = Perspective drawing of [CrCl$_3$(py)$_2$(DMF)] structure determined in this study, B = Perspective drawing of [CrCl$_3$(py)$_2$(DMF)] structure determined by Broomhead [88]**

The pyridine rings are non-planar relative to each other with a difference in corresponding torsion angles of 8.9° (as shown in Figure 2.35) where C(1)–N(1)–Cr(1)–Cl(3) is 50.9(2)° and C(10)– N(2)–Cr(1)–Cl(3) is 42.0(2)°. This twist is noticeably larger than the 1.5° difference observed between the *trans* pyridine ligands in [Hpy][CrCl$_4$(py)$_2$].
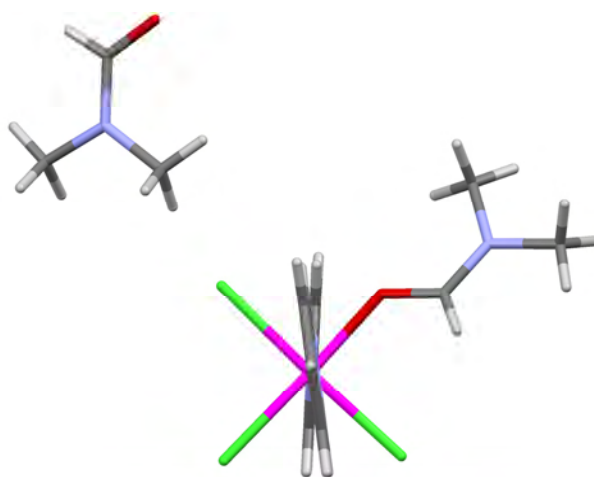
Figure 2.35   **Non-planarity of the *trans* pyridine ligands in [CrCl$_3$(py)$_2$(DMF)]**

A closer look at the metal–ligand bond lengths shows the Cr–Cl and Cr–N bonds correspond well with those of the two structures above. Favourable comparisons are also made with the 'Broomhead structure', with the only noticeable deviation being the shortening and thus strengthening of the equatorial Cr–Cl in the 'Broomhead structure'. This is not observed in the structure of this study and can be explained by the fact that a different ligand environment is *trans* to this particular Cr–Cl bond. This observation highlights the effects that different ligands in different structural orientations have on the properties of other bonds in a complex. To a lesser extent this also had an effect on the bond length of the Cr–O bonds as again that of the 'Broomhead structure' is slightly shorter.

As in the $[CrCl_3(py)_3]$ complex with an encapsulated solvent molecule, no obvious hydrogen bond interactions were observed between the DMF solvate and the metal complex. However, a weak contact (2.795 Å) between a chlorine atom of the complex and a hydrogen atom of the CH_3CN solvent molecule is observed, which may be construed as a weak hydrogen bond.

Table 2.12 highlights all the important metal–ligand bond lengths, as well as those bond angles that infer an octahedral geometry. As in the structures above, the selected torsion angles are relative to the axial chlorine atoms.

Table 2.13 offers details on crystal data and structural refinement, but a full set of crystallographic data is found in the appendix.

Table 2.12   **Selected bond lengths [Å], bond angles [°] and torsion angles [°] for $[CrCl_3(py)_2(DMF)]$**

Cr(1)-O(1)	2.003(2)	Cr(1)-Cl(1)	2.3120(9)
Cr(1)-N(1)	2.102(3)	Cr(1)-Cl(3)	2.3268(9)
Cr(1)-N(2)	2.106(3)	Cr(1)-Cl(2)	2.3277(9)
O(1)-Cr(1)-N(1)	86.98(10)	N(2)-Cr(1)-Cl(3)	90.36(8)

O(1)-Cr(1)-N(2)	88.77(10)	Cl(1)-Cr(1)-Cl(3)	92.12(4)
N(1)-Cr(1)-Cl(1)	92.93(7)	O(1)-Cr(1)-Cl(2)	87.90(7)
N(2)-Cr(1)-Cl(1)	91.33(7)	N(1)-Cr(1)-Cl(2)	89.34(8)
O(1)-Cr(1)-Cl(3)	89.91(7)	N(2)-Cr(1)-Cl(2)	90.83(8)
N(1)-Cr(1)-Cl(3)	89.32(8)	Cl(1)-Cr(1)-Cl(2)	90.06(3)
Cl(3)-Cr(1)-N(1)-C(1)	50.9(2)	Cl(2)-Cr(1)-N(2)-C(10)	140.2(2)
Cl(2)-Cr(1)-N(1)-C(1)	-131.3(2)	Cl(3)-Cr(1)-N(2)-C(6)	141.7(2)
Cl(3)-Cr(1)-N(1)-C(5)	-129.7(2)	Cl(2)-Cr(1)-N(2)-C(6)	-36.1(2)
Cl(2)-Cr(1)-N(1)-C(5)	48.2(2)	Cl(3)-Cr(1)-O(1)-C(11)	-32.2(3)
Cl(3)-Cr(1)-N(2)-C(10)	-42.0(2)	Cl(2)-Cr(1)-O(1)-C(11)	149.0(3)

_____
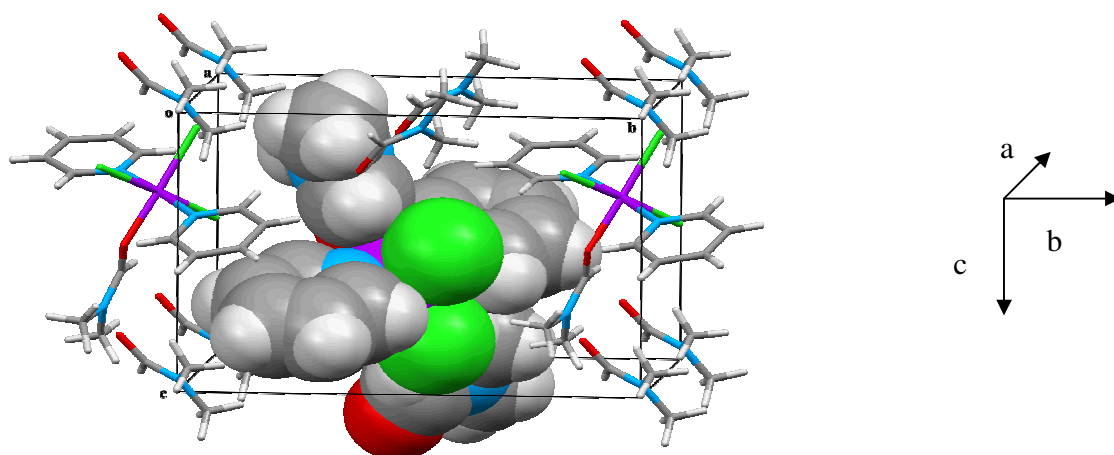
Figure 2.36   **Packing and space fill arrangement of [CrCl$_3$(py)$_2$(DMF)]**

Table 2.13   **Crystal data and structure refinement for [CrCl$_3$(py)$_2$(DMF)]**

_____

Empirical formula	$C_{16} H_{24} Cl_3 Cr N_4 O_2$
Formula weight	462.74
Temperature	293(2) K
Wavelength	0.71073 Å
Crystal system	Monoclinic
Space group	P 2$_1$

|		
Unit cell dimensions	$a = 8.8882(7)$ Å	$\alpha = 90°$
	$b = 13.3255(10)$ Å	$\beta = 94.2880(10)°$
	$c = 9.0420(7)$ Å	$\gamma = 90°$
Volume	$1067.93(14)$ Å^3	
Z	2	
Density (calculated)	1.439 Mg/m^3	
Absorption coefficient	0.928 mm^{-1}	
F(000)	478	
Crystal size	0.26 x 0.18 x 0.06 mm^3	
Theta range for data collection	2.73 to 26.54°.	
Index ranges	-9<=h<=10, -16<=k<=15, -4<=l<=11	
Reflections collected	5 833	
Independent reflections	3 703 [R(int) = 0.0288]	
Completeness to theta = 25.00°	99.6%	
Absorption correction	Semi-empirical from equivalents	
Max. and min. transmission	0.946 and 0.793	
Refinement method	Full-matrix least-squares on F^2	
Data / restraints / parameters	3703 / 1 / 239	
Goodness-of-fit on F^2	1.071	
Final R indices [I>2σ(I)]	R1 = 0.0339, wR2 = 0.0835	
R indices (all data)	R1 = 0.0384, wR2 = 0.0867	
Absolute structure parameter	0.02(2)	
Extinction coefficient	0	
Largest diff. peak and hole	0.247 and -0.218 e.Å^{-3}	

_____

2.4   CATEGORY THREE: PARA–SUBSTITUTED PYRIDINES

The coordination of a variety of electronically and sterically different para-substituent pyridine ligands to the Cr(III) precursor was undertaken with the aim of investigating novel structure–reactivity insights.

In light of the investigations above, three molar equivalents of each ligand were added and only para–substituted pyridine derivatives were used as steric interactions with other ligands / substituents are minimised at this position.

Figure 2.37 highlights the pyridine derivatives that were investigated.
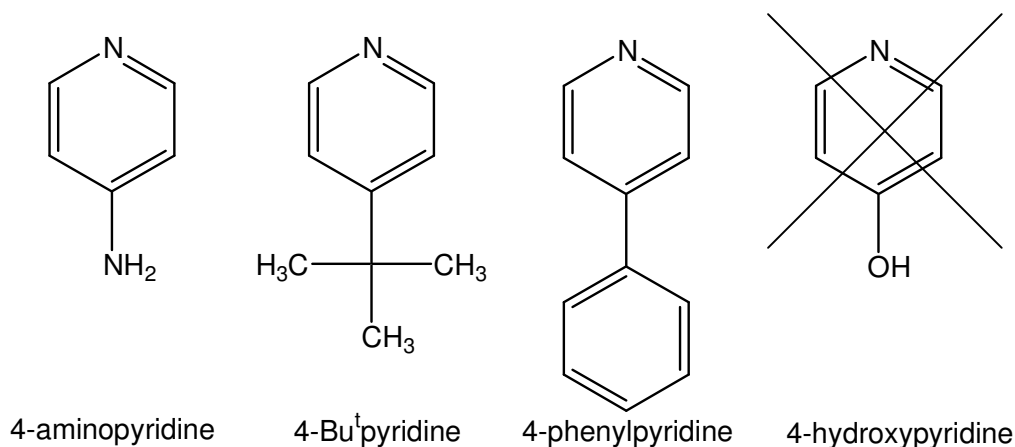
Figure 2.37　　**Para-substituted pyridine ligands**

Only the hydroxy derivative did not yield results as it was insoluble in all workable solvents. The coordination chemistry of the 4–aminopyridine was also of interest as it possesses two nitrogen donor atoms that could coordinate equally through their lone pairs to the metal.

2.4.1　INFRARED AND RAMAN SPECTROSCOPY

The importance of at least one single crystal determination for a class of compounds is clearly illustrated in these pyridine complexes whereby the IR and Raman spectral assignments of precipitates can be made with a degree of confidence.

Detailed vibrational comparisons can be made between the spectra of $[CrCl_3(py)_3]$, $[CrCl_3(py)_2(DMF)]$ and $[CrCl_3(pytb)_3]$ (**7**), with known crystal structures, and the precipitates of $[CrCl_3(pyNH_2)_3]$ (**6**) and $[CrCl_3(pyphenyl)_3]$. Note that as was the case for $[CrCl_3(py)_3]$, spectra were taken of both the single crystal material and the precipitate of $[CrCl_3(pytb)_3]$. The fact that these spectra were identical infers that the single crystal

determination is representative of the bulk precipitate. Of course vibrational differences are expected due to the substituents but there should also be notable similarities.

Furthermore, in the light of the structural determination of [Hpy][CrCl$_4$(py)$_2$] which asks questions about the synthetic route to product formation, IR and Raman spectra are of value.

Evidence of dimeric species in addition to pyridinium–type vibrations is of interest. Although no spectrum of [Hpy][CrCl$_4$(py)$_2$] was obtained due to lack of sample, the presence and absence of bands in these compounds can be compared with the findings of previous literature studies [93, 94, 95] and with the pyH compounds synthesised from the bidentate systems that follow for which spectra were obtained.

With regard to the two spectroscopic techniques themselves, as there is no centre of symmetry in any of the compounds it is expected that all vibrations will be both IR and Raman active [47]. One must be aware, however, that the intensities of the vibrations may differ and a vibration that may seem inactive in either of the two techniques is more than likely simply too weak to be observed. In the following compounds there is a definite trend for the IR vibrations to be stronger than the Raman equivalents.
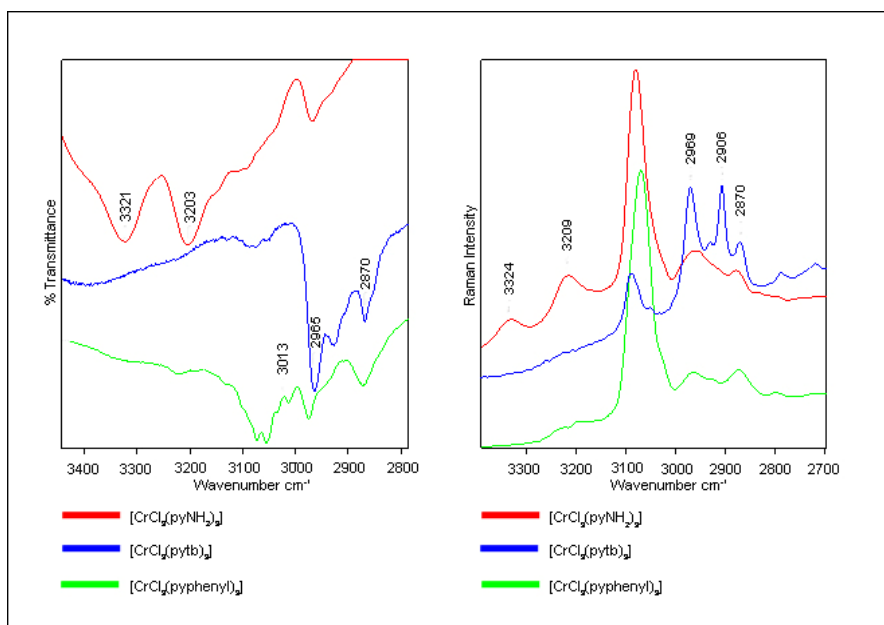
2.4.1.1 Region 3321–2869 cm^{-1}

Common to all three compounds is the presence of C–H pyridine vibrations. In addition, N–H and C–H bands of the respective substituents are also observed.

[CrCl$_3$(pyNH$_2$)$_3$] is the only compound in which bands at 3321 and 3203 cm^{-1} are observed. They are strong vibrations in the IR spectrum but noticeably weaker in intensity in the Raman equivalent. That at 3321 cm^{-1} is confidently assigned to a NH$_2$ asymmetrical stretch vibration which has shifted from its free ligand position of 3300 cm^{-1} [76, 96], thus being an early indication of coordination to the metal. Furthermore, its moderate shift is also an indication that coordination has taken place via the endocyclic pyridine nitrogen and not the nitrogen of the amino group (as both are valid donor

atoms). If that had indeed been the case, a drastic red shift of between 150 and 200 cm^{-1} would have been observed [96]. The other band at 3203 cm^{-1} is assigned the symmetrical NH$_2$ stretching mode [76]. Note also that it is absent in all the other complexes. It is, however, worth mentioning that a pyridinium vibration is expected at this same value [94]. Notably, though, this and one other band are the only evidence, suggesting pyridinium ion formation in the entire spectrum as will be seen in the coming regions.

In the case of the [CrCl$_3$(pytb)$_3$], strong bands in both the IR and Raman spectra at 2965, 2906 cm^{-1} (visible only in the Raman spectrum as in the literature [92]) and 2870 cm^{-1} infer symmetrical and asymmetrical CH$_3$ stretching vibrations [92]. A further symmetrical CH$_3$ stretch is observed only in the Raman spectrum at 2930 cm^{-1}. This is in accordance with the literature [92]. It is more difficult to assign bands specifically to the phenyl substituent of [CrCl$_3$(pyphenyl)$_3$] as the vibrations are very similar to those of pyridine. Note that the opposite of the pytb compound is seen as there is a band at 3013 cm^{-1} visible only in the IR spectrum [97]. Figure 2.38 highlights the important vibrations.

Figure 2.38   **IR and Raman spectra of [CrCl$_3$(pyNH$_2$)$_3$] (red), [CrCl$_3$(pytb)$_3$] (blue), [CrCl$_3$(pyphenyl)$_3$] (green) in the region 3321 – 2869 cm^{-1}**

2.4.1.2 Region 1638–1045 cm^{-1}

This is an interesting region which possesses a combination of ring and C–H vibrations pertaining to the different pyridine derivatives. In all cases there is a strong correlation with the literature in terms of those bands that experience shifts and those that do not, as a consequence of coordination.
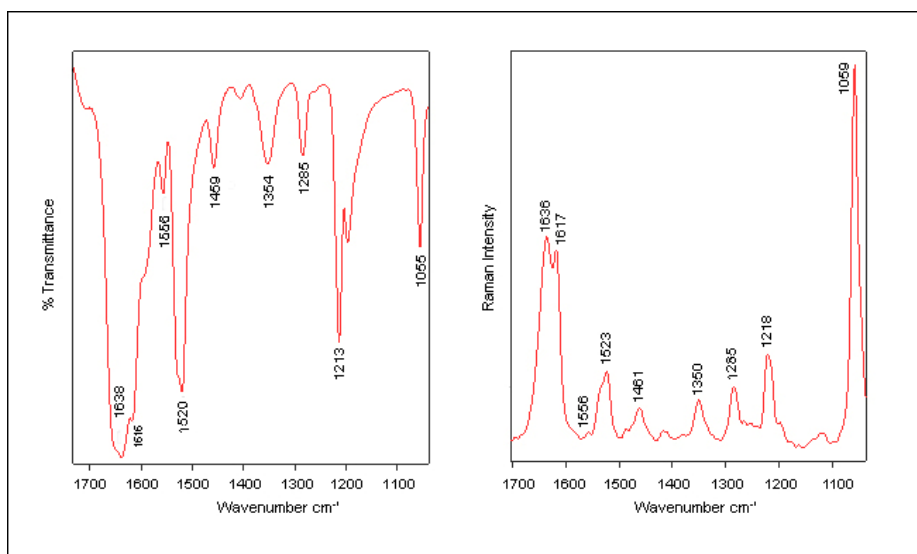
[CrCl$_3$(pyNH$_2$)$_3$]

Two amino-specific vibrations are observed at 1638 (δNH$_2$) and 1285 cm^{-1} (ν C–NH$_2$), where their free ligand positions are 1648 and 1268 cm^{-1} respectively. Both shifts indicate coordination to the metal centre, backed by the literature, even though a downward shift for the δNH$_2$ mode is perhaps surprising as most coordinating shifts are in the opposite direction. The remaining bands, with the exception of 1196 cm^{-1}, are associated with pyNH$_2$ vibrations, with more than half shifting to higher frequencies [96]. Note the comparison between IR and Raman band intensities – IR being predominantly stronger. The vibrational shifts are presented in Table 2.14 while the spectrum is highlighted in Figure 2.39).

Table 2.14   Infrared and Raman band shifts in the region 1638 – 1045 cm^{-1}

Free pyNH$_2$ IR/RAMAN /cm^{-1}	[CrCl$_3$(pyNH$_2$)$_3$]		Shift / cm^{-1} IR/RAMAN
	IR / cm^{-1}	RAMAN / cm^{-1}	
1602	1616sh	1617m	14/15
1556	1556m	1556vw	0
1506	1520s	1523w	14/17
1440	1459m	1461w	19/21
1333	1354m	1350w	21/17
1268	1285m	1285w	17/17
1213	1213s	1218w	0/5
1055	1055s	1059m	0/4

1196 cm^{-1} is more than likely a C–H vibration associated with the pyridine ring, with no shifting observed [92].

Figure 2.39   **IR and Raman spectra of [CrCl$_3$(pyNH$_2$)$_3$] in the region 1638 – 1045 cm^{-1}**

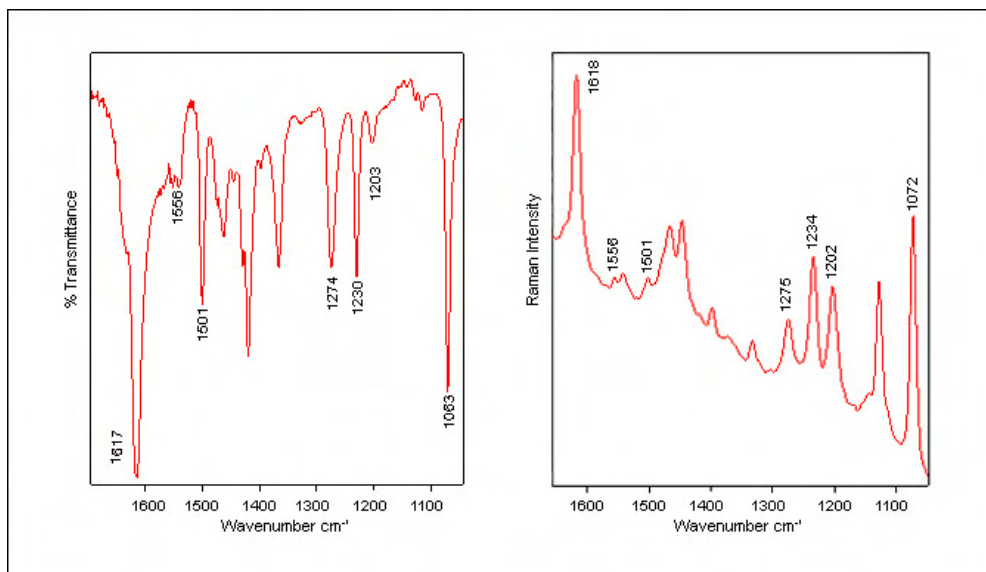### [CrCl$_3$(pytb)$_3$]

All expected ligand vibrations are clearly visible and easily assignable. The five tertiary butyl-specific vibrations exhibit a degree of shifting indicative of metal–ligand coordination and can be assigned to symmetrical (1421 cm^{-1}) and asymmetrical (1475, 1463, 1368 cm^{-1}) CH$_3$ deformations, as well as C–C stretching modes (1128 cm^{-1}).

The remainder are a combination of ring and C–H pyridine vibrations and, as in the amino compound, more than half are shifted to higher frequencies With respect to IR and Raman band intensity, all vibrations correspond well with the literature [92]. The band shifts as well as the spectra are presented in Table 2.15 and Figure 2.40 respectively.

Table 2.15   **IR and Raman band shifts in the region 1638 – 1045 cm^{-1}**

Free pytb IR/RAMAN /cm^{-1}	[CrCl$_3$(pytb)$_3$] IR / cm^{-1}	RAMAN / cm^{-1}	Shift / cm^{-1} IR/RAMAN
1596/1596	1617s	1618m	21/22
1544/1543	1556m	1556vw	12/12
1494/1495	1501s	1501w	7/6
1274/1274	1274s	1275m	0/1
1224/1224	1230s	1234m	6/10
1203/1202	1203m	1202m	0/0
1074/1074	1068s	1072s	-4/-2

Figure 2.40 **IR and Raman spectra of [CrCl$_3$(pytb)$_3$] in the region 1638 – 1045 cm^{-1}**

[CrCl$_3$(pyphenyl)$_3$]

As in the region 3321 to 2869 cm^{-1}, there is difficulty in differentiating between the heterocyclic pyridine and the phenyl vibrations, and a large amount of band superposition is expected. However, it is observed that neither free pyridine nor coordinated pyridine possesses bands at 1514, 1289 and 1045 cm^{-1}, and these are therefore tentatively assigned as phenyl-specific modes. Interestingly, the two former (of three) vibrations are considerably stronger in the Raman spectrum than in the IR spectrum, while the latter band at 1045 cm^{-1} is too weak in the Raman spectrum to be observed.

The only evidence of shifting is observed with the band at 1612 cm^{-1} in the complex that is assignable to coordinated pyridine and has shifted from 1600 cm^{-1} [97]. Both the IR and Raman spectra are presented in Figure 2.41.
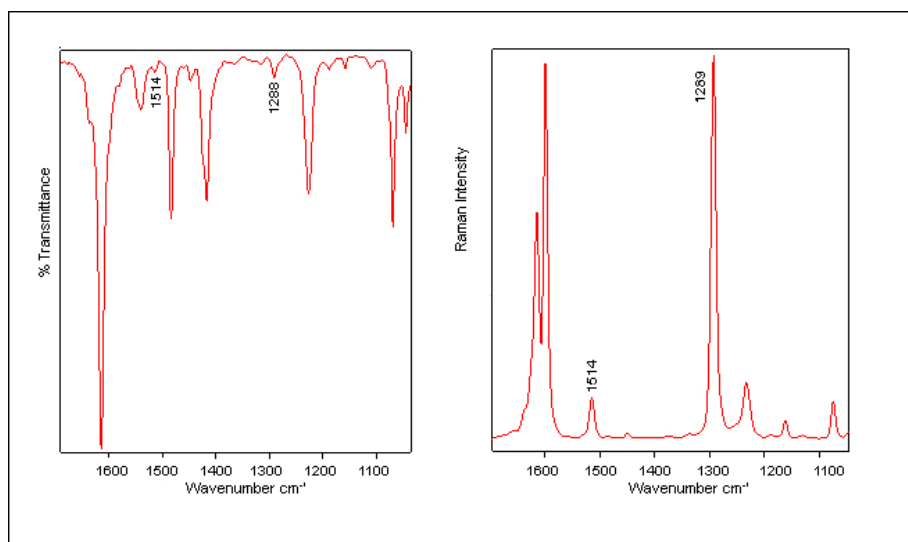
Figure 2.41   **IR and Raman spectra of [CrCl$_3$(pyphenyl)$_3$] in the region 1638 – 1045 cm^{-1}**

2.4.1.3   Region 1030–499 cm^{-1}

This is a region with yet more vibrational evidence associated with both pyridine and the respective para–substituents. In addition, there is also valuable information pertaining to both ligand substitution and the strength of specific bonds.

[CrCl$_3$(pyNH$_2$)$_3$]

Bands associated with both pyNH$_2$ ring and C–H vibrations in accordance with the literature are present. A number of these bands have shifted from the free ligand positions [96] (see Table 2.16). The spectra are presented in Figure 2.42.

Table 2.16   **IR and Raman band shifts in the region 1030 – 499 cm^{-1}**

Free pyNH$_2$ IR / cm^{-1}	[CrCl$_3$(pyNH$_2$)$_3$] IR / cm^{-1}	RAMAN / cm^{-1}	Shift / cm^{-1} IR/RAMAN
991	1022s	1022m	31/31
842	855w	858vs	13/16
824	827s	not visible	3/-
661	667vw	667m	6/-
536	571s	569w	35/33
522	528s	528w	6/-
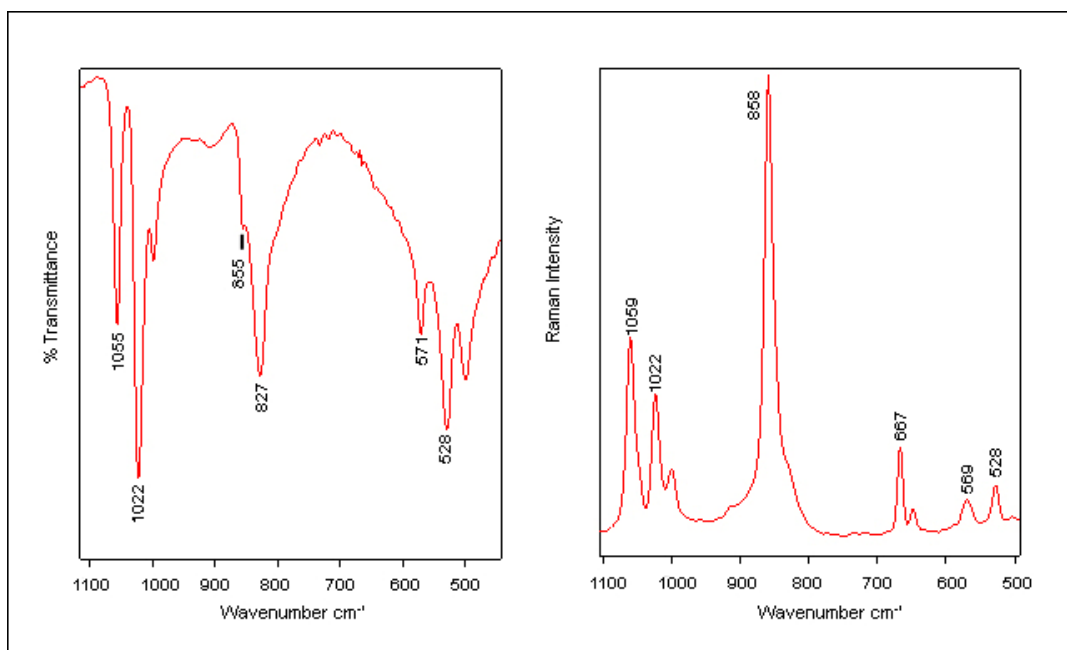
Figure 2.42   **IR and Raman spectra of [CrCl$_3$(pyNH$_2$)$_3$] in the region 1030 – 499 cm^{-1}**

[CrCl$_3$(pytb)$_3$]

As well as the expected pytb ring and C–H vibrations, substituent specific bands at 928 (CH$_3$ rock), (tertiary butyl skeletal stretch) and 548 cm^{-1} (tertiary butyl rock) are present [92]. Vibrational shifts are visible in Table 2.17 while the spectra of [CrCl$_3$(pytb)$_3$] is presented in Figure 2.43.

.

Table 2.17   **IR and Raman band shifts in the region 1030 – 499 cm^{-1}**

Free pytb IR / cm^{-1}	[CrCl$_3$(pytb)$_3$] IR / cm^{-1}	RAMAN / cm^{-1}	Shift / cm^{-1} IR/RAMAN
991	1028s	1028s	37/37
927	928w	931w	1/4
842	844m	844w	2/2
821	831s	not visible	10
711	729m	730s	18/19
669	665w	668m	-4/-1
569	573s	575w	4/6
534	548w	549w	14/15
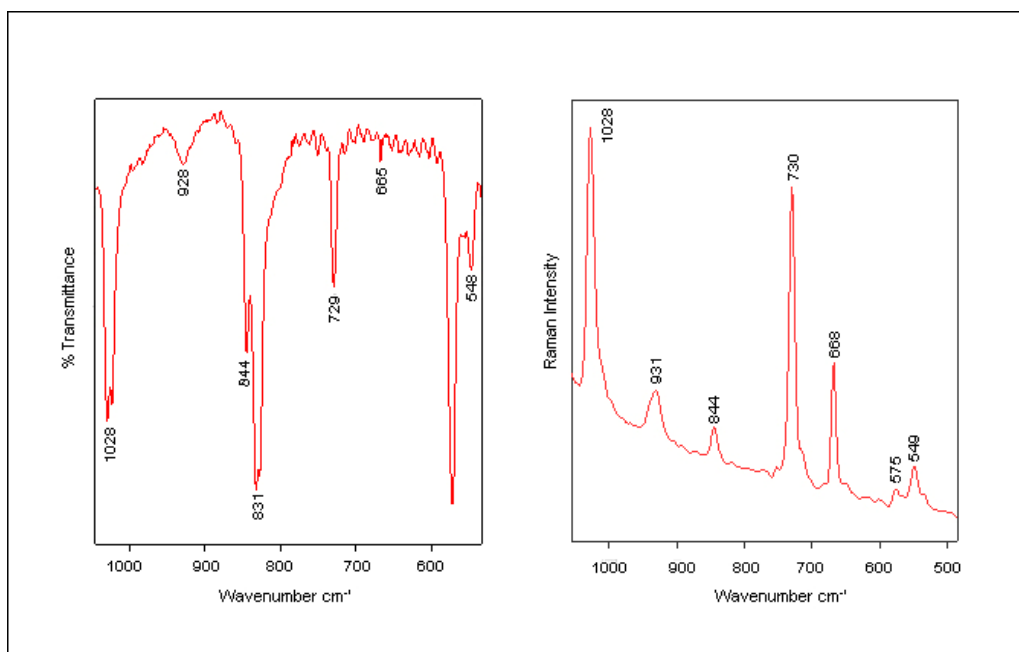
Figure 2.43   IR and Raman spectra of [CrCl₃(pytb)₃] in the region 1030 – 499 cm⁻¹

[CrCl₃(pyphenyl)₃]

As in the previous region, comparative studies allow tentative differentiations between the pyridine and phenyl modes. The bands at 839, 769, 731 and 565 cm^{-1} are assigned to phenyl while the remainder are associated with pyridine [97]. Band shifts and spectra are presented in Table 2.18 and Figure 2.44 respectively.

Table 2.18   IR and Raman band shifts in the region 1030 – 499 cm⁻¹

Free pyphenyl IR / cm^{-1}	[CrCl₃(pyphenyl)₃] IR / cm^{-1}	RAMAN / cm^{-1}	Shift / cm^{-1} IR/RAMAN
1017	1032m	1032s	15/15
991	1012m	1014m	21/23
832	839m	841w	7/9
762	769s	760m	7/-2
731	731m	not visible	0
687	694m	not visible	7
608	625s	617w	17/9
561	565m	564w	4/3

73
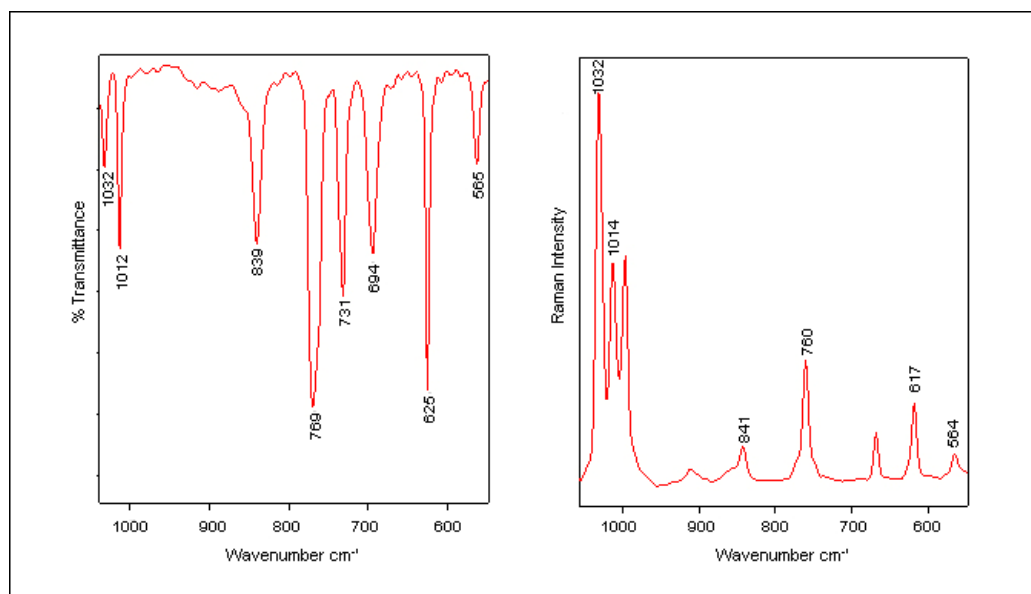
Figure 2.44   IR and Raman spectra of [CrCl₃(pyphenyl)₃] in the region 1030 – 499 cm⁻¹

2.4.1.4   Ligand substituents

Here the importance of analysing a compound of known crystal structure is exemplified, in this case [CrCl$_3$(pytb)$_3$]. One of the strongest indications of coordinated thf from the [CrCl$_3$(thf)$_3$] precursor is a strong band at around 856 cm^{-1} and its presence in these compounds would be indicative of partial substitution of thf ligands. All three compounds possess a band in and around this region at 855 (pyNH$_2$), 844 (pytb) and 839 cm^{-1} (pyphenyl), yet they can be confidently assigned to respective ligand vibrations [92, 96, 97, 98].

What the spectrum of a known crystal structure does is rule out ambiguity in assignments. Note that the amino complex is the only one of the three where the Raman vibration is stronger than the IR.

2.4.1.5   Bond strength

According to Topacli and Bayari [75] there is much information to be gained from the shifting of pyridine ring vibrations to higher frequencies upon coordination to the chromium centre. The extent to which the pyridine vibrations shift once coordinated to the metal can be correlated to the mass, nature, number and position of the various

pyridine substituents and can be explained as the coupling of the internal modes of the aromatic molecule with the metal–nitrogen (M–N) vibrations [75]. The data to date show that the majority of the ring vibrations are indeed shifted to higher frequencies upon coordination. The band in and around 990 cm^{-1} is a characteristic pyridine ring breathing band. It is also present in the para–substituted derivatives. If one considers the mass of the substituents, one notices the correlation between increasing mass and shifting of this band. The smallest substituent by mass is the amino group, which has bands at 997 and 1022 cm^{-1}. When compared with the free $pyNH_2$ ligand, it is clear that the former is a $pyNH_2$-specific band shifted from 949 cm^{-1}, while the latter at 1022 cm^{-1} is the characteristic ring breathing mode. The next largest is the tertiary butyl group with a band at 1028 cm^{-1} and the largest is the phenyl group with a band at 1030 cm^{-1}. The phenyl also has a band at 1012 cm^{-1}, but this was initially assigned to a C–H band associated with the para-positioning [97]. Once again, the value of crystal structural data combined with spectroscopy is highlighted as studies discussed in Chapter 4 will reveal that in fact 1011 cm^{-1} has shifted from 991 and 1030 cm^{-1} is a C–H vibration of the pyphenyl ligand, probably shifted from 1017 cm^{-1}. The band at 997 cm^{-1} in the Raman spectrum is assigned to a trigonal ring breathing mode of the phenyl ring [113]. These shifts are highlighted in Table 2.19 and Figure 2.45.

Table 2.19   **Shifting of the characteristic ring breathing vibration in [CrCl$_3$py$_3$],**
[CrCl$_3$(pyNH$_2$)$_3$], [CrCl$_3$(pytb)$_3$] and [CrCl$_3$(pyphenyl)$_3$]

Pyridine / cm^{-1}	[CrCl$_3$py$_3$] / cm^{-1}	Shift / cm^{-1}
990s	1014m	24

pyNH$_2$ / cm^{-1}	[CrCl$_3$(pyNH$_2$)$_3$] / cm^{-1}	Shift / cm^{-1}
991s	1022	31

pytb / cm^{-1}	[CrCl$_3$(pytb)$_3$] / cm^{-1}	Shift / cm^{-1}
995vs	1028	33

pyphenyl / cm^{-1}	[CrCl$_3$(pyphenyl)$_3$] / cm^{-1}	Shift / cm^{-1}
1001s	1011	10

The substituents also have an effect on the strength of the metal–nitrogen bonds. In fact, the order of the M–N ligand stretching vibrations reflects the increasing strength of the M–N bond. Therefore, as well as the mass effects, the increase in charge density on the pyridine ring brought about by the various electronic effects of the substituents is also influential. The concept of releasing charge density into the ring and thereby increasing the electron density on the nitrogen atom has the effect of strengthening the M–N bond [75]. One would expect the amino group, as the strongest electron-donating group, to exhibit the greatest shift, followed by the phenyl and tertiary butyl groups which release similar charges into the pyridine ring, with the unsubstituted pyridine complex shifting the least. This is not entirely reflected in the recorded spectra although what is interesting is that similar results were found when investigating the three pyridine derivatives coordinating to other metal compounds [75, 92, 96, 97].

It was suggested that the small shifts in the 4–aminopyridine compound may be due to hydrogen bonding of the NH_2 group [75]. Furthermore, the fact that $[CrCl_3(pyNH_2)_3]$ in particular exhibits these shifts also allows one to conclude that it is the endocyclic nitrogen lone pair that is involved in metal coordination as opposed to the amino group nitrogen [96] (supported by the N–H stretching vibrations discussed earlier).
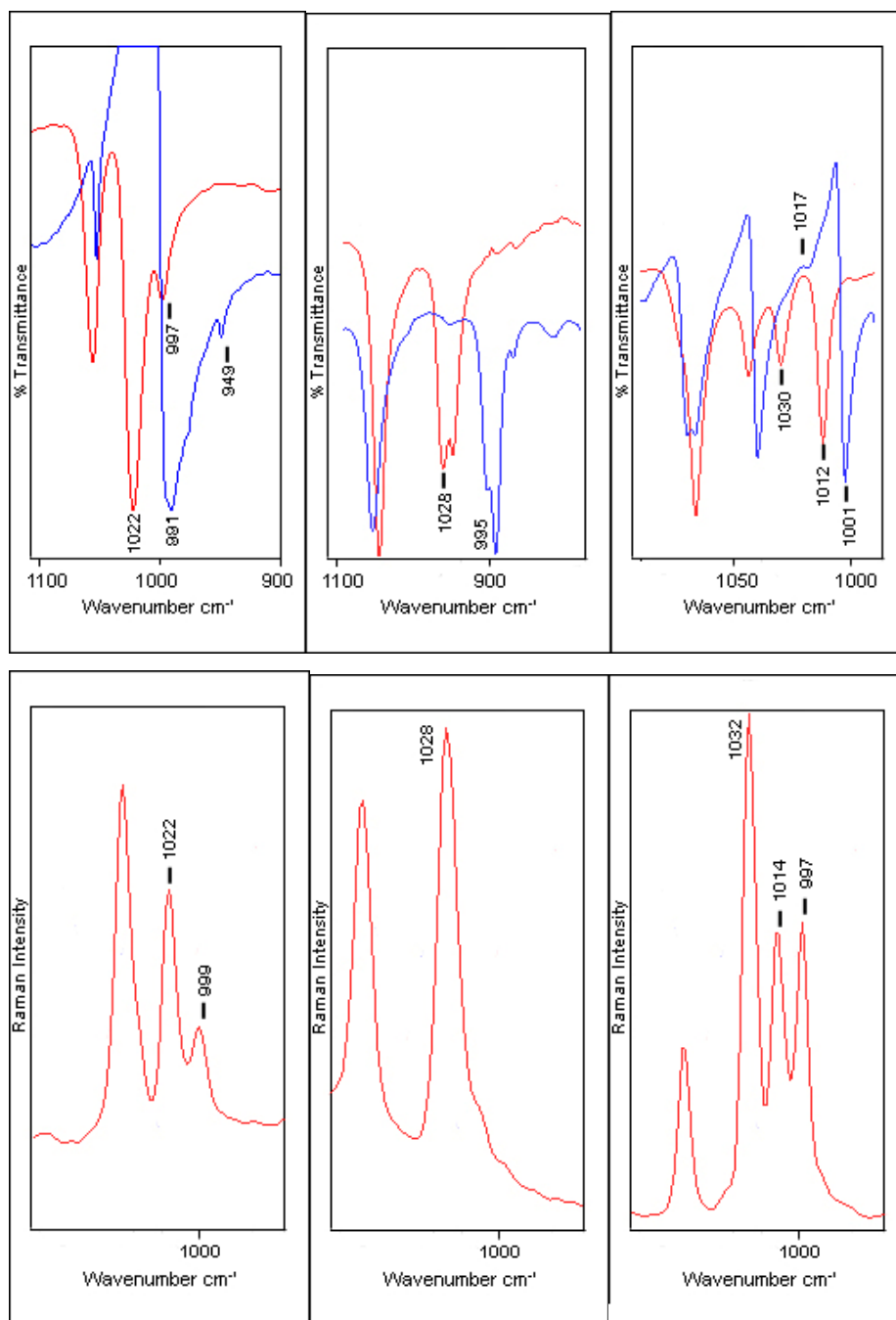
Figure 2.45 **Shifting of the characteristic ring breathing vibration in the IR spectra of [CrCl$_3$(pyNH$_2$)$_3$], [CrCl$_3$(pytb)$_3$] and [CrCl$_3$(pyphenyl)$_3$], relative to free ligand positions (blue). Raman spectra of [CrCl$_3$(pyNH$_2$)$_3$], [CrCl$_3$(pytb)$_3$] and [CrCl$_3$(pyphenyl)$_3$]**

The effects of the substituents are not limited to the pyridine ring vibrations. The FIR spectra of metal–pyridine compounds assigns the band in and around 221 cm^{-1} to the Cr–

N stretch vibration [41, 80, 81]. Therefore the presence of this band is most certainly a strong indication that the substitution of the thf ligands has taken place and the pyridine is now coordinated to the chromium centre. It must be noted that this band is metal-sensitive and the value of 221 cm^{-1} defines Cr–N bonds specifically. The literature suggests that this band shifts to lower frequencies as the mass of the substituent on the pyridine ligand increases [81]. With respect to the pyridine compounds at hand, where expected, downward shifting has occurred. However, apart from the $[CrCl_3(py)_3]$ compound with an expected band at 221 cm^{-1}, only the pytb compound has a single decisive band in this region. This band is at 213 cm^{-1}, which conforms to the literature suggestion [81]. The amino and phenyl spectra are less clear as they both possess bands at 219 and 213 cm^{-1}. One would expect the shift of both these substituents to be of a similar if not greater (especially the bulky phenyl) magnitude than pytb, hence the value of 213 cm^{-1} is more sensible. However, when one compares these values with those in section 1 of the bipyridine compounds, it can be seen that it was in fact the phenyl that shifted the most, with the tertiary butyl and amino showing no shifting. It is therefore clear that the environment of the ligands must be taken into account and one cannot simply rely on the mass of substituents for definitive shifts.

2.4.1.6 Region 488–213 cm^{-1}

It is in the FIR spectra where a great deal of interest lies as the presence of metal–ligand vibrations confirm coordination. The three bands indicative of Cr–Cl vibrations in the *mer* arrangement are duly present in all the compounds [80]. This also implies that the precipitates are monomeric as pyridinium-type species such as $[Hpy][CrCl_4(py)_2]$ would have shown four Cr–Cl bands in accordance with both the literature [99] and the data presented in the later chapters.

An interesting band, which is unassignable in terms of the literature, is that at 268 cm^{-1}. The fact that it is present in all three substituted pyridine compounds and not in the unsubstituted pyridine compound may lead one to infer that it stems from a para–position substituent effect. Moreover, the possibility of the band being indicative of Cr–O [82] and thus coordinated thf was ruled out as the band is also present in $[CrCl_3(pytb)_3]$.The effects

of the substituents are not limited to the pyridine ring vibrations. The FIR spectra of metal–pyridine compounds assign the band in and around 221 cm^{-1} to the Cr–N stretch vibration [41, 80, 81]. Therefore the presence of this band is most certainly a strong indication that substitution of the thf ligands has taken place and the pyridine is now coordinated to the chromium centre. It must be noted that this band is metal-sensitive and the value of 221 cm^{-1} defines Cr–N bonds specifically. The literature suggests that this band shifts to lower frequencies as the mass of the substituent on the pyridine ligand increases [81]. With respect to the pyridine compounds at hand, where expected, downward shifting has occurred. However, apart from the [CrCl$_3$(py)$_3$] compound with an expected band at 221 cm^{-1}, only the pytb compound has a single decisive band in this region. This band is at 213 cm^{-1}, which conforms to the suggestion in the literature [71]. The amino and phenyl spectra are less clear as they both possess bands at 219 and 213 cm^{-1}. One would expect the shift of both these substituents to be of a similar magnitude to, if not greater (especially the bulky phenyl) than, the tertiary butyl, hence the value of 213 cm^{-1} is more sensible. However, when these values are compared with those of the bipyridine compounds, it is apparent that it was in fact the phenyl that shifted the most, with the tertiary butyl and amino showing no shifting. It is therefore clear that the environment of the ligands must be taken into account and one cannot simply rely on the mass of the substituents for definitive shifts.

2.4.1.7   Concluding remarks

All of the vibrational frequencies of the pyridine and substituted pyridine compounds have been compared with the structures in this study published by Brennan [100] and are discussed later in Chapter 3, which includes one equivalent of these ligands along with bipyridine in the compounds. As expected, the relevant bands were all present except for the CH$_3$ rocking vibration of the pytb compound at 927 cm^{-1} [92]. The correlation between the FIR bands was also made with the confirmation of the Cr–Cl bands and the Cr–N bands (see Section 2.4 for Cr–N detail).

Table 2.20 **Vibrational assignments of [CrCl$_3$(py)$_2$DMF] (5), [CrCl$_3$(pyNH$_2$)$_3$] (6), [CrCl$_3$(pytb)$_3$] (7) and [CrCl$_3$(pyphenyl)$_3$] (8)**

5	6		7		8		Assignment
IR / cm^{-1}	IR / cm^{-1}	RAMAN / cm^{-1}	IR / cm^{-1}	RAMAN / cm^{-1}	IR / cm^{-1}	RAMAN / cm^{-1}	
-	3321s	3324w	-	-	-	-	ν(NH$_2$) asym (76, 96)
-	3203s	3209w	-	-	-	-	ν(NH$_2$) sym (76, 96)
3114w, 3080w, 3050w, 3032w	3092s	3082m	3081m	3088m	3072m	3073m	ν(CH) (97, 73, 74, 96, 92)
-	-		-	-	3013m	-	ν(CH) (97)
3000w, 2940w	-	-	-	-	-	-	ν(CH of CH$_3$ - DMF) (87)
2804w, 2871w	-	-	-	-	-	-	ν(CH) of carbonyl - DMF (87)
-	-	-	-	-	2977m	2982vw	unassigned
-	-	-	2965vs	2969s	-	-	ν (CH$_3$) asym (92)
-	-	-	-	2930w	-	-	ν (CH$_3$) sym (92)
-	2966s	2961w	-	-	-	-	unassigned
-	-	-	-	2906m	-	-	ν (CH$_3$) sym (92)
-	-	-	2870s	2870m	-	-	ν (CH$_3$) sym (92)
-	-	-	-	-	2873m	2873w	unassigned
1660vs, 1649vs	-	-	-	-	-	-	ν(C=O) of carbonyl (88)
-	1638s	1636m	-	-	-	-	δ(NH$_2$) (26)
1606s	1616sh	1617m	1617vs	1618vs	1612vs	1614m,1600vs	ν_{ring} (97, 73, 74, 96, 92)
-	1556m	1556vw	1556w	1556w	1539m	-	ν_{ring} (97, 73, 74, 96, 92)
-	1520s	1523w	1501m	1501w	1514vw	1514m	ν_{ring} (97, 96, 92)
1485m	-	-	-	-	1483s	1483vw	ν_{ring} (97, 73, 74)

5	6		7		8		Assignment
-	-	-	1475m	-	-	-	(CH$_3$) asym def (92)
-	1459m	1461w	1463m	1466m	-		ν_{ring} (97, 96)
1447s	-	-	1446w	1446m	-	-	(CH$_3$) asym def (92) / ν_{ring} (73, 74)
1433s	-	-	-	-	-	-	δ(CH$_3$) - DMF (87)
-	-	-	1421s	1420vw	-	-	(CH$_3$) sym def (92)
-	-	-	-	-	1417s	1407vw	δ(CH) (97)
1391m	-	-	-	-	-	-	δ(NCH) carbonyl (87)
-	-	-	1368m	1371vw	-	-	(CH$_3$) asym def (92)
1360s	1354m	1350w	-	-	-	-	ν_{ring} (96)
-	-	-	-	-	1288w	1289vs	ν_{ring} + δ(CH) (97)
-	1285m	1285w	-	-	-	-	ν(C-NH$_2$) (96)
-	-	-	1274m	1275m	-	-	δ(CH) (92)
1247m	-	-	-	-	-	-	ν(C-N) asym of N(CH$_3$)$_2$ (87)
-	-	-	1230m	1234m	1227s	1232m	δ(CH) (97, 82)
1219s	1213s	1218w	-	-	-	-	δ(CH) (96)
-	1196m	1197w	1203w	1202m	-	-	δ(CH) / ν (CC) (97, 96)
1163w, 1152w	-	-	-	-	1160vw	1160m	δ(CH) (97, 73, 74)
1126m	-	-	1128w	1128m	-	-	ν (CC) (92) / CH$_3$ def – DMF (91)
1095m	-	-	-	-	-	-	γ(CH$_3$) - DMF (89)
1071m	-	-	1068s	1072s	1070s	1074m	δ(CH) (96) / ν_{ring} (97)
-	1055s	1059m	-	-	-	-	δ$_{ring}$ (96)

5	6		7		8		Assignment
1045m	-	-	-	-	1045m	-	ν_{ring} (97) / γ (CH$_3$) - DMF (89)
-	-	-		-	1030m	1032s	δ(CH) (97)
1015m	1022s	1022m	1028m	1028s	1012m	1014m	Ring breathing (pyX) (97, 73, 74, 96, 92)
-	997m	999m	-	-	998vw	997m	Trigonal ring breathing (phenyl ring) (114) / pyNH$_2$ vib (96)
978w, 948w	-	-	-	-	-	-	γ(CHO) op - DMF (87)
-	-	-	928w	931w	-	-	(CH$_3$) rock (92)
-	855w	858vs	-	-	-	-	X-sens (96, 98)
-	827s	-	844m, 831s	844w	839m	841w	py breathing (92)
765s	-	-	-	-	769s	760m	δ_{ring} + ν_{ring} (97)
-	-	-	729m	730s	731m	-	γ_{ring} def (92) / γ(CH) (97)
693s	-	-	-	-	694m	-	γ_{ring} (97)
658m	667vw	667m	665w	668m	-	-	δ_{ring} (96) / ν (CC) (92)
644s	-	-	-	-	-	-	δ_{ring} (73, 74)
-	-	-	-	-	625s	617w	δ_{ring} (97)
-	571s	569w	573s	575w	565m	564w	skeletal str (92)
-	-	-	548w	548w	-	-	rock (tb) (92)
-	528s	528w	-	-	-	-	X-sens (96)
-	499s	501vw	-	-	-	-	unassigned
448m	-	-	-	-	488m	-	δ_{ring} (97, 73, 74)
415m	414vw	412m	-	-	-	-	γ_{ring} (96)
-	-	-	-	-	406w	404m	γ_{ring} (96)

5	6		7		8		Assignment
397m, 390s	-	-	399w	399w	-	-	CCC def (tb) (92) / (CNC) def - DMF (91, 92)
358m	352m	-	371s	369w	366s	365m	Cr – Cl (80)
324m	334m	332w	353m	352w	355s	-	Cr – Cl (80)
302m	312m	-	326m	327w	331s	331w	Cr – Cl (80)
-	-	-	-	-	301w	305w	unassigned
284m, 230m	-	-	-	-	-	-	Cr - O
-	268w	270m	268m	265s	266s	263m	para - py
-	219w	216sh	-	-	219w	-	Cr – N (py) (41, 80, 81)
214	213w	-	213w	-	214w	213w	Cr – N (py) (41, 80, 81)

ν = stretching, δ = in plane bending, γ = out of plane bending, def = deformation, asym = asymmetric, sym = symmetric vs = very strong, s = strong, m = medium, w = weak, vw = very weak

2.4.2   COMPUTATIONAL STUDIES

Of the three substituent pyridine complexes, $[CrCl_3(pyNH_2)_3]$ and $[CrCl_3(pytb)_3]$ were selected as representative examples for computational study. This decision was reached on the basis of the more distinctive substituent vibrations, coupled with the fact that pyphenyl compounds have been selected for computational studies in the later chapters. A further reason for choosing $[CrCl_3(pytb)_3]$ was that its crystal structure has been determined.

For the most part, the experimental spectra correlate very well with their calculated equivalents in both complexes. Note that as a result of the same solid-state effects that were highlighted for the calculated IR spectrum of $[CrCl_3(py)_3]$ in Figure 2.10, the FIR spectra of these two complexes are not shown.

$[CrCl_3(pyNH_2)_3]$

With respect to the characteristic N–H and C–H stretching vibrations expected above 3000 cm^{-1}, the strongest correlation between experimental and calculated frequencies is seen in the IR spectra. However, as can be seen in Figures 2.46 and 2.47, the rest of the mid–vibrational region shows good frequency matches in both the IR and Raman spectra.
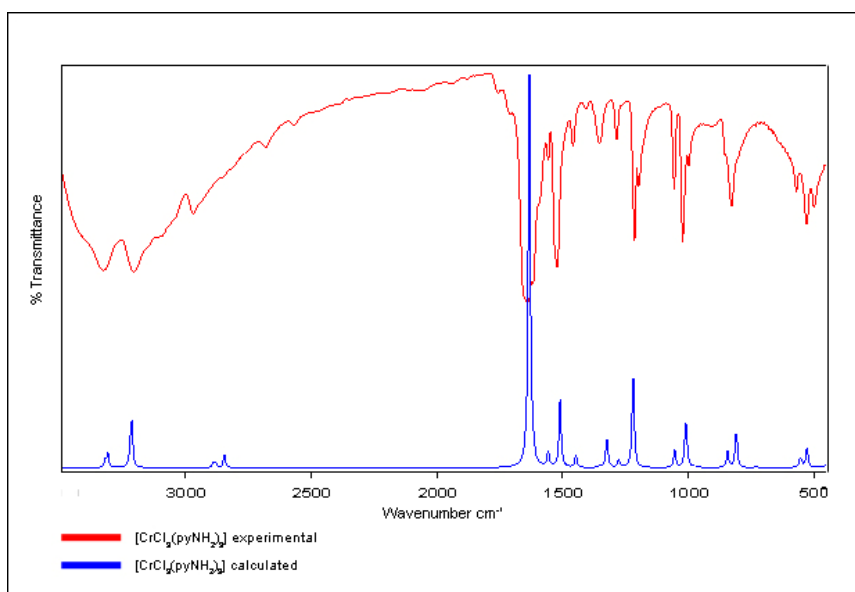
Figure 2.46   **Experimental (red) and calculated (blue) MIR spectra of $[CrCl_3(pyNH_2)_3]$**
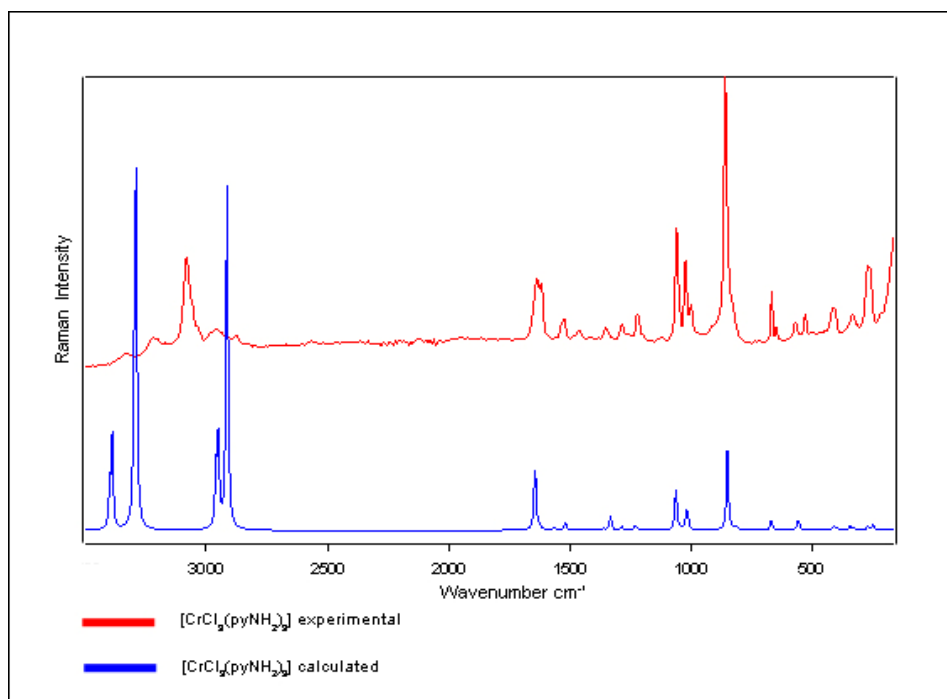
Figure 2.47   **Experimental (red) and calculated (blue) Raman spectra of [CrCl$_3$(pyNH$_2$)$_3$]**

Selected vibrations of importance have been documented in Table 2.21. The N–H vibrations are of interest as the literature assignments of asymmetrical and symmetrical stretching modes are confirmed by the computational data. The much-discussed ring breathing mode of pyridine is also of importance as the calculated values help to confirm that this has resulted from the shifting of the free pyridine vibration at ~992 cm^{-1}.

The FIR spectra metal–ligand vibrations correspond reasonably well, bearing in mind the expected solid state effects. Interestingly, the calculated Cr–N vibration is found at approximately the same value as in [CrCl$_3$(py)$_3$], which is higher than that found in the literature [41, 80, 81].

Table 2.21   **Selected experimental and calculated IR and Raman band assignments for**
     [CrCl$_3$(pyNH$_2$)$_3$]

[CrCl$_3$(pyNH$_2$)$_3$] IR / cm^{-1}		[CrCl$_3$(pyNH$_2$)$_3$] Raman / cm^{-1}		Assignment	
Experimental	Calculated	Experimental	Calculated	Experimental	Calculated
3321	3310	3324	3391	ν(NH$_2$) asym	ν(NH$_2$) asym
3203	3214	3209	3292	ν(NH$_2$) sym	ν(NH$_2$) sym
1638	1637	1636	1643	δ(NH$_2$)	δ(NH$_2$) + ν_{ring}
1285	1278	1285	1286	ν(C-NH$_2$)	C-NH$_2$ rock + ν_{ring}
1022	1011	1022	1018	Ring breathing (pyNH$_2$)	Ring breathing (pyNH$_2$)
352, 334, 312	343, 337	332	345, 339, 247	Cr-Cl	Cr-Cl
	327	-	329	-	NH wag
219, 213	295	216	297	Cr-N	Cr-N

ν = stretching, δ(NH$_2$) = scissoring

Table 2.22   **Scaling factors determined for [CrCl$_3$(pyNH$_2$)$_3$]**

Region / cm^{-1}	IR	Raman
0 – 1878	0.974597	0.980275
2980 – 3909	0.894264	0.916082

Unlike the unsubstituted tri–pyridine complex, both the HOMO and LUMO orbitals that were generated are centred on the chlorine atoms (Figure 2.48), which is a direct result of the resonance effects associated with amino-substituted delocalised systems.
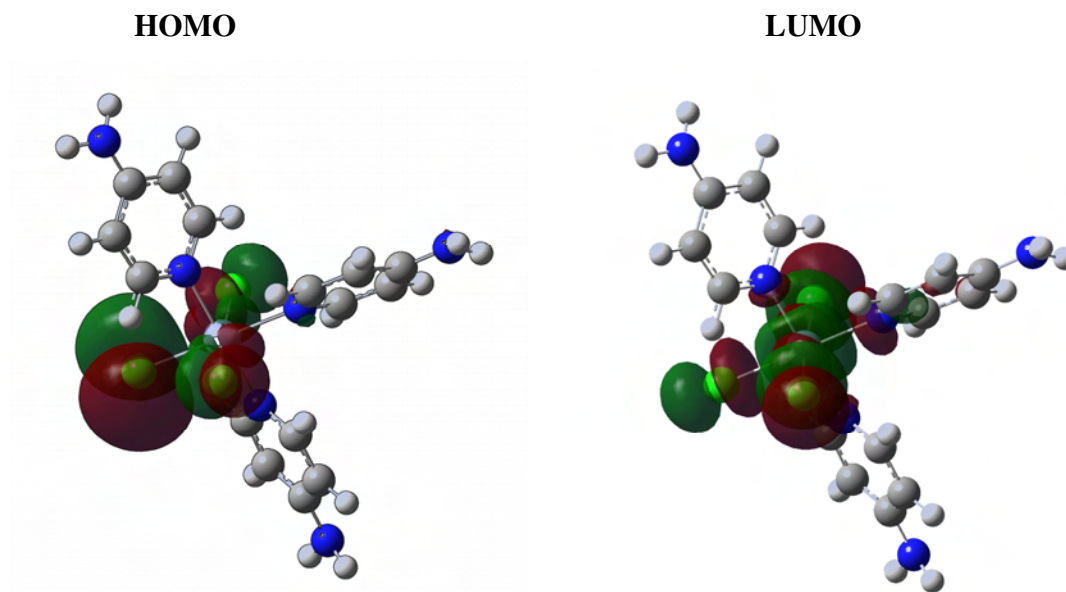
HOMO   **LUMO**

Figure 2.48   HOMO and LUMO orbitals of [CrCl$_3$(pyNH$_2$)$_3$]

[CrCl$_3$(pytb)$_3$]

As illustrated in Figures 2.49 and 2.50, there is an excellent agreement between the experimental and calculated spectra.

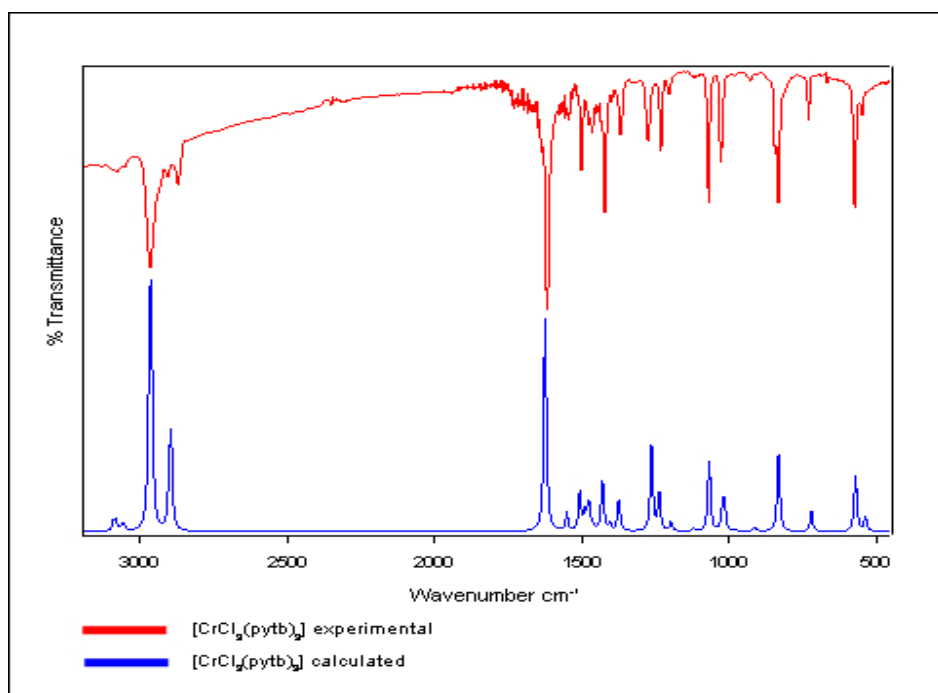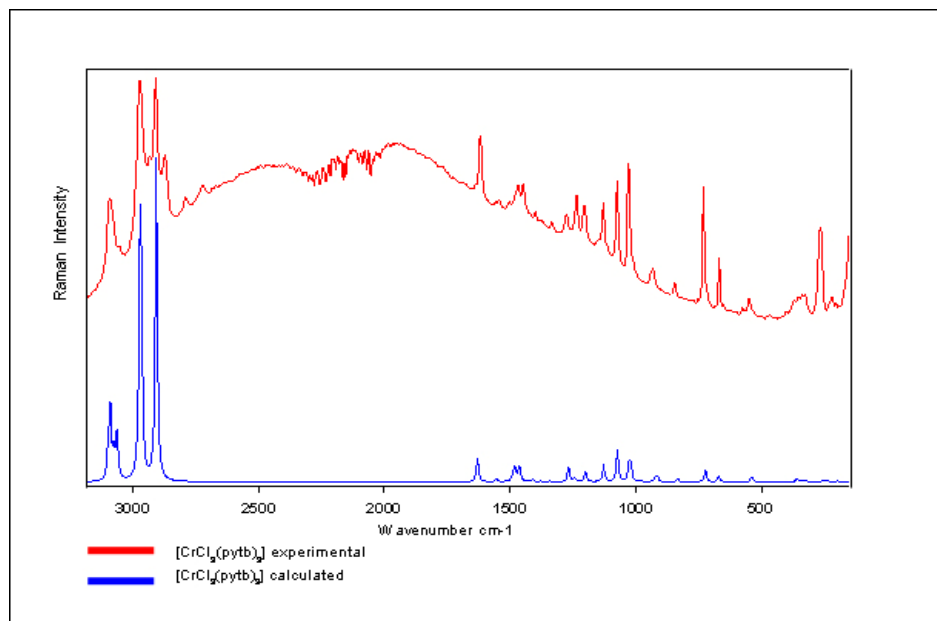**Figure 2.49   Experimental (red) and calculated (blue) MIR spectra of [CrCl$_3$(pytb)$_3$]**

Figure 2.50   Experimental (red) and calculated (blue) Raman spectra of [CrCl$_3$(pytb)$_3$]

Characteristic substituent, ring and metal–ligand vibrations indicative of coordination are highlighted in Table 2.23. Of these, the calculated metal–ligand modes are the hardest to identify as many of the frequencies are a combination of modes.

Table 2.23   Selected experimental and calculated IR and Raman band assignments for [CrCl$_3$(pytb)$_3$]

| [CrCl$_3$(pytb)$_3$] IR / cm^{-1}		[CrCl$_3$(pytb)$_3$] Raman / cm^{-1}		Assignment	
Experimental	Calculated	Experimental	Calculated	Experimental	Calculated
2965	2965	2969	2968	ν(CH$_3$) asym	ν(CH$_3$) asym
2870	2895	-	-	ν(CH$_3$) sym	ν(CH$_3$) sym
1617	1624	1618	1628	ν_{ring}	ν_{ring}
1368	1374	1371	1376	CH$_3$ asym def	CH$_3$ sym def
1029, 1023	1020	1028	1024	Ring breathing (pytb)	Ring breathing (pytb) + CH$_3$ wag
371, 353, 326	360, 352, 344	369, 352, 327	360, 354, 343	Cr-Cl	Cr-Cl + pytb rock + Cr-N
-	-	-	325	-	Pytb rock

88

-	322	-	325	-	Cr-Cl + CH$_3$ twist
268	276	265	276	Para py	Cr-N + CH$_3$ twist
213	262	-	-	Cr-N	Cr-N + CH$_3$ twist

Table 2.24   Scaling factors determined for [CrCl$_3$(pytb)$_3$]

Region / cm^{-1}	IR	Raman
0 - 1861	0.978328	0.980529
2826 - 3433	0.956048	0.957495

The nature of the tertiary butyl substituents reveals, as expected, HOMO and LUMO orbitals similar to those found in [CrCl$_3$(py)$_3$], with the chlorine atoms being rich in electron density and thus susceptible to electrophilic attack. Likewise, the *trans* chlorine ring system is electron-deficient due to being found on a polarised axis and is thus open to attack by nucleophilic species. See Figure 2.51.

HOMO   **LUMO**
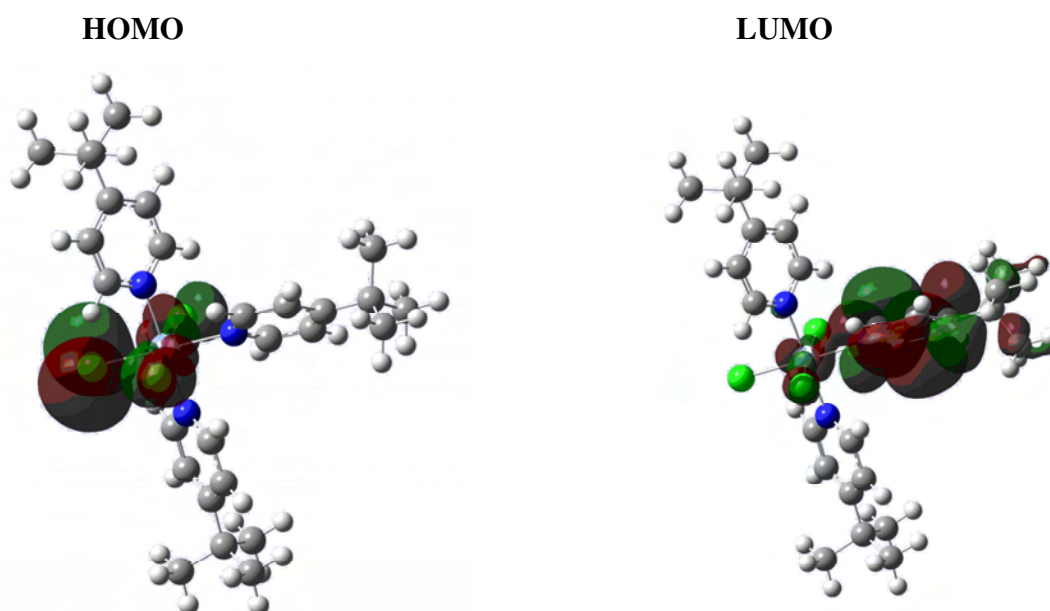
Figure 2.51   HOMO and LUMO orbitals of [CrCl$_3$(pytb)$_3$]

2.4.3 ^{1}H NMR OF [CrCl$_3$(thf)$_3$] AND THREE EQUIVALENTS OF PYPHENYL

The in situ ^{1}H NMR reaction study that followed the addition of three equivalents of unsubstituted pyridine to [CrCl$_3$(thf)$_3$] to yield [CrCl$_3$(py)$_3$] was repeated for the tri–para substituted para–phenylpyridine complex. The method and reaction conditions were unchanged, with acetone–d$_6$ remaining the solvent of choice. The resulting spectra are depicted in Figure 2.52 and show that after 173 minutes all pyphenyl resonances have disappeared, which infers complete coordination to the paramagnetic metal centre.

One had perhaps expected phenyl vibrations to remain present upon completion of the reaction on the basis that they are sufficiently far away from the paramagnetic centre, but this was not the case.
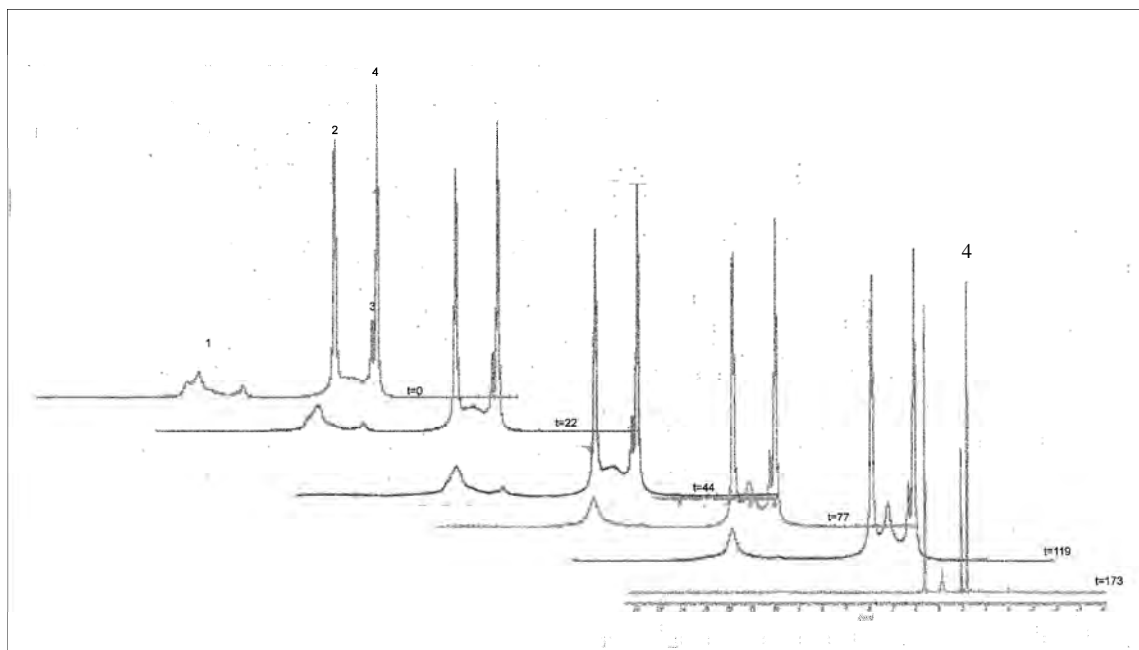
Figure 2.52   **Stacked ^{1}H NMR spectra for the reaction of pyphenyl with [CrCl$_3$(thf)$_3$] over time.**
     1 = pyphenyl, 2 = thf, 3 = acetone-d$_6$, 4 = thf

2.4.4 MASS SPECTROMETRY

The FAB-MS of the [CrCl$_3$(pyphenyl)$_3$] precipitate is shown in Figures 2.53 and 2.54 and discussed as a representative example of the three substituted pyridine complexes. The isotopic distribution patterns of a number of fragments associated with the precipitate

90

sample of $[CrCl_3(pyphenyl)_3]$ were observed. These included the molecular ion, $[M]^+$ (m/z = 625), in addition to $[M–Cl]^+$ (m/z = 587), $[M–pyphenylCl]^+$ (m/z = 432) and $[M–pyphenylCl_2]^+$ (m/z = 397). All patterns were in agreement with the theoretically generated equivalents.
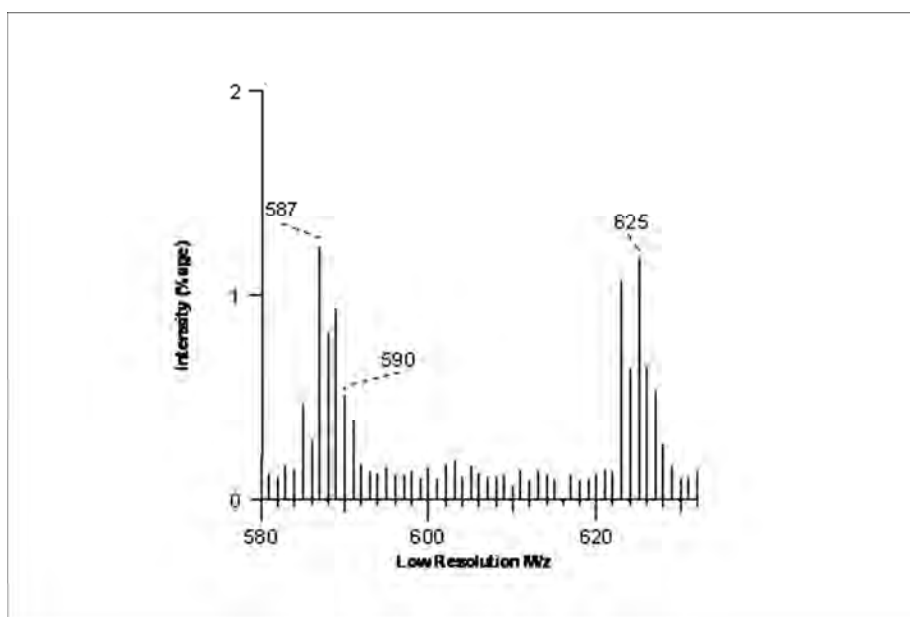

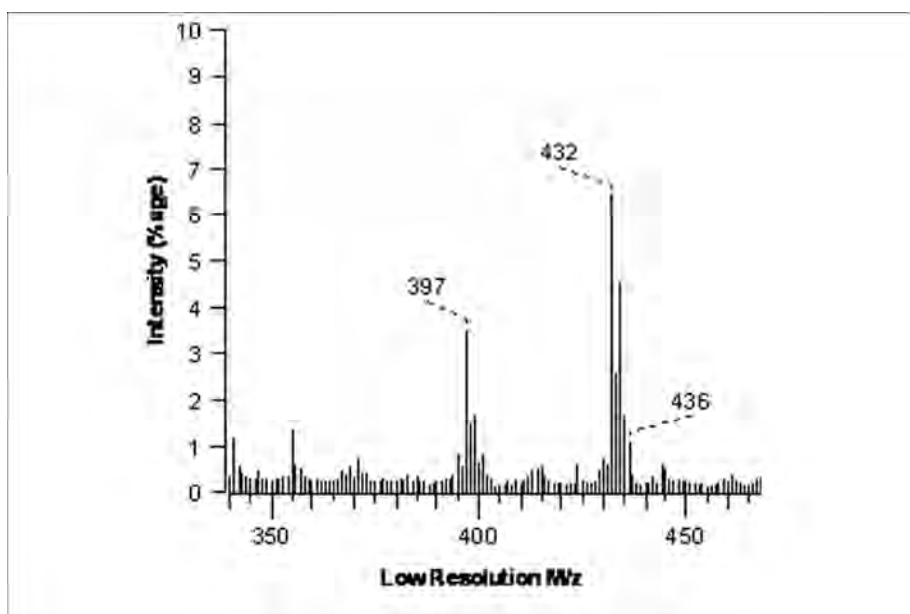**Figure 2.53   FAB-MS spectrum of $[CrCl_3(pyphenyl)_3]$**

Figure 2.54   FAB-MS spectrum of $[CrCl_3(pyphenyl)_3]$

2.4.5   X-RAY CRYSTALLOGRAPHY

2.4.5.1   [CrCl₃(pytb)₃]

The single crystals of $[CrCl_3(pytb)_3]$ were isolated from the reaction mixture of the three equivalents of pytb added to $[CrCl_3(thf)_3]$ in thf that had been allowed to stir at room temperature overnight. The resulting dark green supernatant was left to stand and after 3 days dark green plate–like crystals were observed. Crystallographic data was then able to reveal the novel structural determination of $[CrCl_3(pytb)_3]$. A perspective drawing of the determined structured is shown in Figure 2.55.
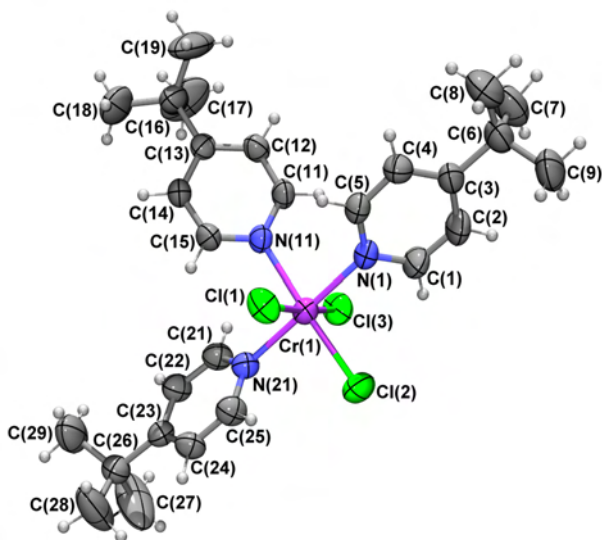
**Figure 2.55   Perspective drawing of [CrCl₃(pytb)₃] structure determined**

The molecular structure of $[CrCl_3(pytb)_3]$ is an interesting variant on both the unsubstituted equivalent $[CrCl_3(py)_3]$ ([83] and this study) and the ethyl equivalent reported by Modec [101] known as *mer*–trichloro–tris(4–ethylpyridine)chromium(III), $[CrCl_3(pyEt)_3]$. Comparisons in terms of bond lengths, bond angles and torsion angles are of interest in order to gauge the effect of increasing the steric bulk of the ligand. In addition, a particularly interesting feature observed solely in the lattice packing arrangement of $[CrCl_3(pytb)_3]$ will also be discussed.

The chromium atom is coordinated to three chlorine atoms and three nitrogen atoms of the pytb ligands in a *mer* arrangement. What appear to be two disordered hexane and thf molecules are also found within the unit cell.

The coordination is approximately octahedral, with the largest deviation being the Cl(1)-Cr(1)–Cl(2) bond angle (93.73(4)°). All the other *cis* X–Cr–Y bond angles are in the range 86.58(7)–92.41(4)°.

As in all the analogous structures the ring systems are non–planar. However, it is observed that the [CrCl$_3$(py)$_3$] structure determined in this study is the only structure in which the pyridine ligands twist anti–clockwise relative to the axial chlorine atoms. A clockwise twist is seen in the other structures, including this novel [CrCl$_3$(pytb)$_3$] structure. Figure 2.56 clearly shows the clockwise twisting of the aromatic systems relative to the axial chlorine atoms.
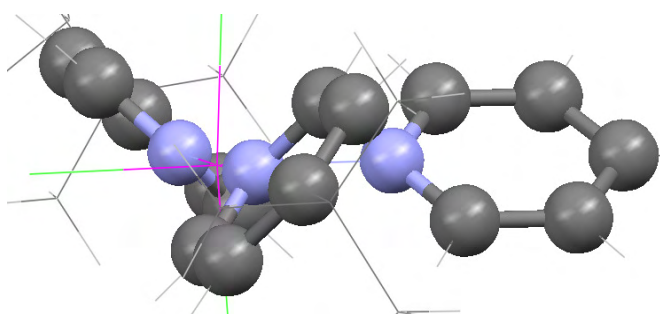
Figure 2.56   **Twisting of the aromatic systems relative to the axial chlorine atoms in**
                    [CrCl$_3$(pytb)$_3$]

A comparison between the metal–ligand bond lengths of unsubstituted ethyl and tertiary butyl pyridines showed very little variation. It should also be noted that the disordered solvent molecules did not interact via hydrogen bonding with the complex. Table 2.25 gives the equivalent bond length, bond angle and torsion angle data highlighted in the three structures above while Table 2.26 gives the crystal and structural refinement data.

Table 2.25   Selected bond lengths [Å], bond angles [°] and torsion angles [°] for [CrCl₃(pytb)₃]

_____

Cr(1)-N(1)	2.105(2)	Cr(1)-Cl(2)	2.3056(9)
Cr(1)-N(21)	2.105(2)	Cr(1)-Cl(1)	2.3248(9)
Cr(1)-N(11)	2.130(2)	Cr(1)-Cl(3)	2.3263(9)

N(1)-Cr(1)-N(11)	88.03(9)	N(11)-Cr(1)-Cl(1)	87.32(7)
N(21)-Cr(1)-N(11)	92.08(9)	Cl(2)-Cr(1)-Cl(1)	93.73(4)
N(1)-Cr(1)-Cl(2)	89.49(7)	N(1)-Cr(1)-Cl(3)	91.18(7)
N(21)-Cr(1)-Cl(2)	90.44(7)	N(21)-Cr(1)-Cl(3)	90.55(7)
N(1)-Cr(1)-Cl(1)	89.70(7)	N(11)-Cr(1)-Cl(3)	86.58(7)
N(21)-Cr(1)-Cl(1)	88.57(7)	Cl(2)-Cr(1)-Cl(3)	92.41(4)

Cl(1)-Cr(1)-N(1)-C(5)	-39.8(2)	Cl(1)-Cr(1)-N(11)-C(11)	126.7(2)
Cl(3)-Cr(1)-N(1)-C(5)	134.1(2)	Cl(3)-Cr(1)-N(11)-C(11)	-54.4(2)
Cl(1)-Cr(1)-N(1)-C(1)	141.9(3)	Cl(1)-Cr(1)-N(21)-C(25)	-49.2(2)
Cl(3)-Cr(1)-N(1)-C(1)	-44.3(3)	Cl(3)-Cr(1)-N(21)-C(25)	136.9(2)
Cl(1)-Cr(1)-N(11)-C(15)	-53.7(2)	Cl(1)-Cr(1)-N(21)-C(21)	126.3(2)
Cl(3)-Cr(1)-N(11)-C(15)	125.2(2)	Cl(3)-Cr(1)-N(21)-C(21)	-47.5(2)

_____

Symmetry transformations used to generate equivalent atoms:
#1 y+1/3,-x+y+2/3,-z+2/3   #2 x-y+1/3,x-1/3,-z+2/3

Table 2.26   Crystal data and structure refinement for [CrCl₃(pytb)₃]

_____

Empirical formula	$C_{30} H_{46} Cl_3 Cr N_3 O_{0.5}$
Formula weight	615.05
Temperature	293(2) K
Wavelength	0.71073 Å
Crystal system	Trigonal
Space group	R 3
Unit cell dimensions	a = 33.3142(14) Å α = 90°

	b = 33.3142(14) Å	β = 90°
	c = 15.6483(13) Å	γ = 120°
Volume	15040.3(15) Å^3	
Z	18	
Density (calculated)	1.222 Mg/m^3	
Absorption coefficient	0.606 mm^{-1}	
F(000)	5 832	
Crystal size	0.32 x 0.18 x 0.14 mm^3	
Theta range for data collection	2.45 to 26.58°	
Index ranges	-41<=h<=41, -40<=k<=41, -6<=l<=19	
Reflections collected	27 543	
Independent reflections	6 532 [R(int) = 0.0405]	
Completeness to theta = 25.00°	99.9%	
Absorption correction	Semi-empirical from equivalents	
Max. and min. transmission	0.919 and 0.784	
Refinement method	Full-matrix least-squares on F^2	
Data / restraints / parameters	6 532 / 0 / 381	
Goodness-of-fit on F^2	1.064	
Final R indices [I>2σ(I)]	R1 = 0.0502, wR2 = 0.1264	
R indices (all data)	R1 = 0.0758, wR2 = 0.1423	
Extinction coefficient	0	
Largest diff. peak and hole	0.388 and -0.289 e.Å^{-3}	

_____

Perhaps the most interesting aspect of this novel structure was the lattice packing arrangement. As can be seen in Figures 2.57 and 2.58 there are two distinct cavities or channels, with the larger of the two accommodating a molecule of the thf solvent.
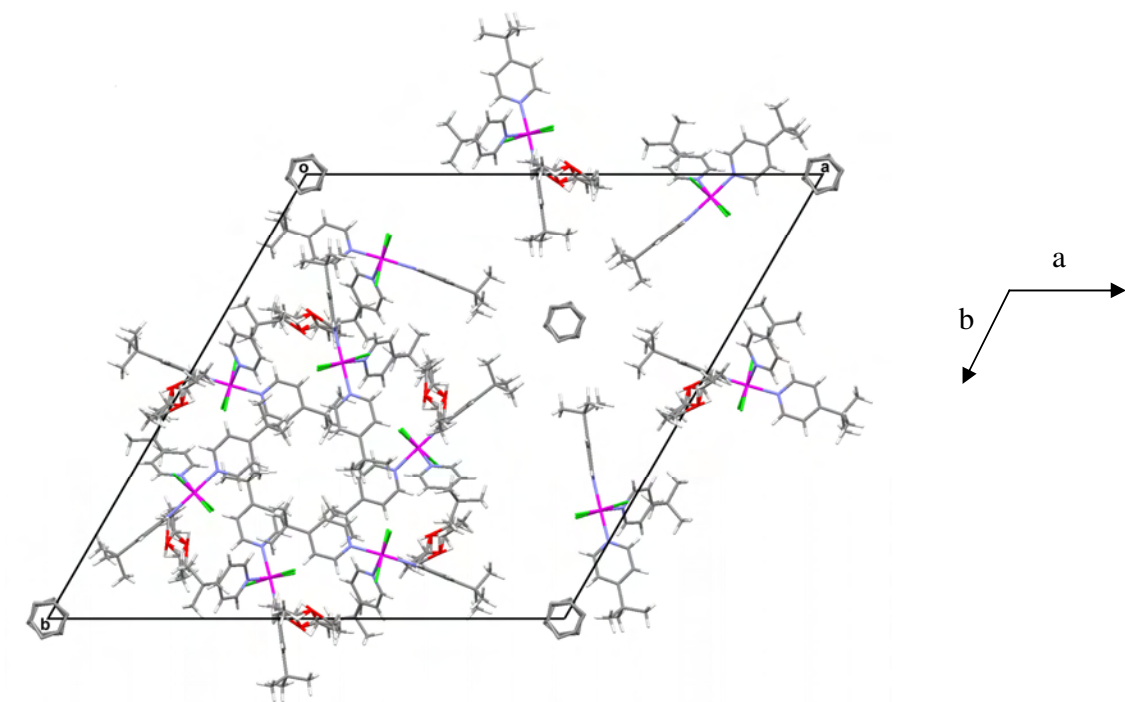
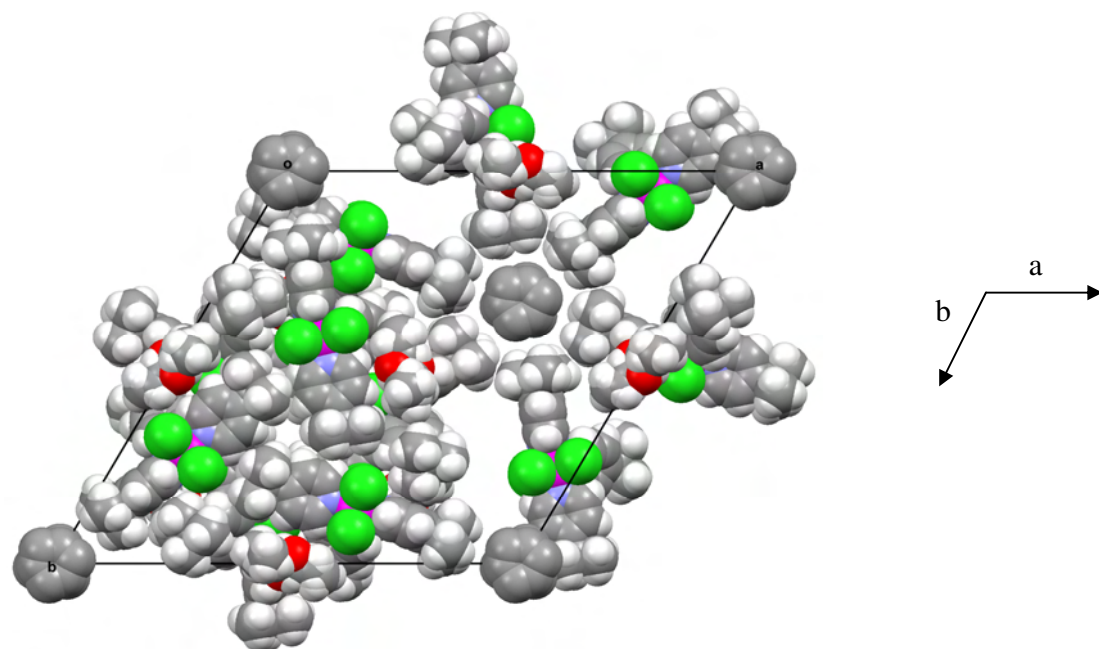**Figure 2.57** **Packing arrangement of [CrCl₃(pytb)₃]**

Figure 2.58 **Space fill representation of the packing arrangements**

This then opened the way for further experimentation with respect to being able to vary the encapsulated molecule by varying the reaction solvent. This, however, was not a straightforward task. The problem in choosing a solvent was that it had to solubilise the metal precursor in the reaction, as well as being of suitable size to be accommodated by the cavity. One was also wary of solvents that could potentially coordinate to the metal centre which would lead to unwanted competition for the available sites. This has already been observed in the compound $[CrCl_3(py)_2(DMF)]$ and will also be seen in later chapters.

After many different solvents had been investigated, the best choice appeared to be dioxane. As well as having the correct solubility, it is also of similar size and shape to the thf molecule. Unfortunately, the inability to grow single crystals of suitable size for structural data collection did not allow confirmation of dioxane encapsulation within the cavity.

In the light of the previous results given in this chapter, one must assume that this neutral monomeric compound was formed either from direct ligand substitution or by the symmetrical cleavage of the dimeric intermediate.

2.5   EXPERIMENTAL

2.5.1   SYNTHESIS OF $[CrCl_3(py)(thf)_2]$ (1) AND $[CrCl_3(py)_2(thf)]$ (2)

As stated above, these reactions yielded $[CrCl_3(py)_3]$ as product. Crystals supposedly of $[CrCl_3(py)_2(thf)]$ were grown in CH_3CN, with structural determination confirming the compound $[CrCl_3(py)_3]$.

Schlenk tubes were charged with $[CrCl_3(thf)_3]$ (0.19 g, 0.507 mmol and 0.17 g, 0.454 mmol respectively) and thf (20 cm^3). One and two molar equivalents of pyridine (0.04 ml and 0.07 ml) were added to the respective reaction solutions, affording immediate light green solutions and precipitates. The reactions were stirred overnight and after the same work-up as above (Et$_2$O 3 x 20 cm^3 and dried under reduced pressure),

yielded good yields of product (one equivalent of pyridine: 0.15 g, 75% (**1**), two equivalents of pyridine: 0.16 g, 89% (**2**)).

2.5.2 SYNTHESIS OF [CrCl$_3$(py)$_3$] (3)

A Schlenk tube was charged with [CrCl$_3$(thf)$_3$] (0.23 g, 0.614 mmol) and pyridine (30 cm^3), where pyridine was both reagent and solvent. The reaction was stirred at room temperature overnight to ensure completion. The supernatant was removed and the remaining residue washed with Et$_2$O (3 x 20 cm^3) and dried under reduced pressure for 3 hours to afford an olive green precipitate (**3**) in good yield (0.20 g, 83%).

Crystals of (**3**) were grown from the slow evaporation of a CH$_3$CN solution. The reaction was repeated in a NMR tube to follow the reaction course and profile. Acetone-d$_6$ was the solvent used. Refer to NMR chapter for details. After a period of 5 days, dark green plate–like crystals large enough for the diffractometer were formed in the NMR tube. Structure determination gave the compound [pyH][CrCl$_4$(py)$_2$] (**4**).

2.5.3 SYNTHESIS OF [CrCl$_3$(2,6-dibromopy)$_3$] AND [CrCl$_3$(py)$_2$(DMF)] (5)

Up to this point all substituents were at the para position of the pyridine as coordination to the metal centre was guaranteed not be affected by steric hindrance. However, test reactions were carried out using an ortho–substituted pyridine to ensure that they could not indeed be utilised as a result of their bulkiness at a position too close to the proposed Cr–N coordination site. In the case of the attempted synthesis of [CrCl$_3$(thf)$_3$] plus 3 molar equivalents of 2, 6-dibromopyridine the expected result of no reaction was the case. However, a second experiment was carried out where by both pyridine and 2, 6-dibromopyridine were combined in a Schlenk tube with [CrCl$_3$(thf)$_3$] resulting in an interesting crystal structure of [CrCl$_3$(py)$_2$(DMF)].

A Schlenk tube was charged with [CrCl$_3$(thf)$_3$] (0.23 g, 0.614 mmol) and thf (20 cm^3). Followed by the addition of one molar equivalents of 2,6-dibromopyridine (0.14 g, 0.614 mmol), 2,6-dimethylpyridine (0.06 g, 0.614 mmol) and unsubstituted pyridine (0.05 cm^3). All three ligands were added simultaneously to ensure equal competition for sites. To

ensure completion the reaction was stirred overnight at room temperature. The supernatant was removed via syringe and the residue washed with Et_2O (3 x 20 cm^3). The residue was then dried under reduced pressure for 3 hours yielding (0.21 g, 87%). The crystallisation of the recovered product was limited to DMF and DMSO as solvents due to the insolubility in all other solvents. Dark green plate–like crystals of **(5)** were formed from DMF after approximately 10 weeks.

2.5.4   SYNTHESIS OF [CrCl$_3$(pyNH$_2$)$_3$] (6)

Varying the electronic effects of the ligands was achieved by introducing pyNH$_2$ as the ligand.

A Schlenk tube was charged with [CrCl$_3$(thf)$_3$] (0.25 g, 0.667 mmol) and thf (20 cm^3). On immediate addition of the pyNH$_2$ (0.19 g, 2.001 mmol) the solution turned green and a green precipitate was visible. The reaction was stirred overnight at room temperature. The supernatant was removed after the residue had been allowed to settle. It was subsequently washed with Et_2O (3 x 20 cm^3) and dried under reduced pressure for 3 hours to afford a light green precipitate **(6)** in good yield (0.24 g, 83%).

2.5.5   SYNTHESIS OF [CrCl$_3$(pytb)$_3$] (7)

With the success of the [CrCl$_3$(py)$_3$] compound, the steric effects of the ligands were varied by introducing pytb in place of pyridine.

A Schlenk tube was charged with [CrCl$_3$(thf)$_3$] (0.26 g, 0.0694 mmol) and thf (20 cm^3). Three equivalents of pytb (0.26 cm^3, 2.082 mmol) were then added and the reaction was monitored. It was noted that on immediate addition of the pytb, the reaction mixture turned dark green. The reaction was stirred at room temperature overnight to ensure completion. As no precipitate formed, the green supernatant was reduced under pressure to leave behind an oil–like green substance. Et_2O (10 cm^3) was then added which forced out an olive green precipitate. This ether-based supernatant was removed and after 3 days of standing at room temperature afforded dark green platelet crystals of [CrCl$_3$(pytb)$_3$].

The green precipitate was washed again in Et$_2$O (3 x 20 cm^3) and then dried under reduced pressure to leave an olive green precipitate **(7)** in good yield (0.24 g, 62%).

2.5.6   SYNTHESIS OF [CrCl$_3$(pyphenyl)$_3$] (8)

The steric bulk of the ligands was increased further with the addition of pyphenyl ligands. A Schlenk tube was charged with [CrCl$_3$(thf)$_3$] (0.22 g, 0.587 mmol) and dissolved in thf (20 cm^3). Three equivalents of pyphenyl (0.27 g, 1.761 mmol) were then added, turning the supernatant green and affording a green precipitate. To ensure completion, the reaction was stirred at room temperature overnight. The green supernatant was removed via syringe and the residue washed with Et$_2$O (3 x 20 cm^3), followed by drying of the residue under reduced pressure. An olive green precipitate **(8)** remained in good yield (0.21 g, 58%).

2.5.7   SYNTHESIS OF [CrCl$_3$(pyOH)$_3$]

With the idea of continuing the theme of varying the electronic properties of the coordinating ligands, it was hoped to synthesise [CrCl$_3$(pyOH)$_3$]. However, this was not possible as the pyOH ligand was insoluble in all workable solvents.